

Field-Effect Sensors – From pH sensing to Biosensing: Sensitivity Enhancement using Streptavidin-Biotin as a Model System

Benjamin M. Lowe^a, Kai Sun^a, Ioannis Zeimpekis^a, Chris-Kriton Skylaris^b, Nicolas G. Green^a

so Received 00th January 20xx,
Accepted 00th January 20xx

DOI: 10.1039/x0xx00000x

www.rsc.org/

Field-Effect Transistor sensors (FET-sensors) have been receiving increasing attention for biomolecular sensing over the last two decades due to their potential for ultra-high sensitivity sensing, label-free operation, cost reduction and miniaturisation. Whilst the commercial application of FET-sensors in pH sensing has been realised, their commercial application in biomolecular sensing (termed BioFETs) is hindered by poor understanding of how to optimise device design for highly reproducible operation and high sensitivity. In part, these problems stem from the highly interdisciplinary nature of the problems encountered in this field, in which knowledge of biomolecular-binding kinetics, surface chemistry, electrical double layer physics and electrical engineering is required. In this work, a quantitative analysis and critical review has been performed comparing literature FET-sensor data for pH-sensing with data for sensing of biomolecular streptavidin binding to surface-bound biotin systems. The aim is to provide the first systematic, quantitative comparison of BioFET results for a single biomolecular analyte, specifically Streptavidin, which is the most commonly used model protein in biosensing experiments, and often used as an initial proof-of-concept for new biosensor designs. This novel quantitative and comparative analysis of the surface potential behaviour of a range of devices demonstrated a strong contrast between the trends observed in pH-sensing and those in biomolecule-sensing. Potential explanations are discussed in detail and surface-chemistry optimisation is shown to be a vital component in sensitivity-enhancement. Factors which can influence the response, yet which have not always been fully appreciated, are explored and practical suggestions are provided on how to improve experimental design.

Introduction

Chemical sensors are important in a wide range of applications such as medical diagnostics¹, explosives detection², food safety³ and environmental monitoring⁴. A promising class of chemical sensors are Field-Effect Transistor-sensors (FET-sensors). FET-sensors have been receiving increasing interest over the last two decades, motivated by the need for low-cost biosensors capable of direct and rapid detection of analyte molecules without the need for expensive and time-consuming labelling steps. As a medical diagnostic tool, this would increase survival rates of patients by reducing load on centralised-diagnostic facilities. FET-sensors have the potential to offer ultrahigh sensitivity, low-cost production, portability and facile miniaturisation as part of a 'Lab-on-a-Chip'. FET-sensors present several advantages in comparison with currently available label-free biosensors which operate via mass-detection^{5,6}, the electrical detection offered by FET-sensors provides additional information on, for example, conformational changes⁷ or extracellular potentials⁸. In contrast

to many other biosensing methodologies, FET-sensors do not require bulky optical measurement equipment.

FET-based pH sensors were initially popularised as far back as the 1970s with the work of Bergveld^{9,10}, and have been successfully commercialised¹¹. However, the extension of these devices to sensitive and reliable detection of biomolecular analytes ('BioFET' devices) has proved more difficult than initially expected. These problems have resulted in research providing a range of novel FET-sensor architectures^{12–14} and methods of operation^{15–17}, however advances in the field of BioFET research are obstructed by a lack of consensus on which quantitative metrics (i.e. figure-of-merit) should be used to compare devices. As a result, most published studies can only be compared qualitatively. By focusing on a single biomolecule analyte, this review provides the first comprehensive quantitative analysis of the FET-sensor response. Streptavidin-sensing was primarily chosen as a model system due to its general wide spread usage and well-understood (bio)chemistry. This is compared with pH sensing, which is a better understood application of FET sensors, and has already been well-characterised. This review also highlights factors that can influence the response yet have not always been fully appreciated, thereby resulting in sub-optimal experimental design.

One particular design aspect in pH sensing using FET-sensors^{18–20} is that the oxide material plays a dominant role in determining the magnitude of the response. An important

^a Department of Electronics and Computer Science, Nano Research Group, University of Southampton, UK.

^b School of Chemistry, University of Southampton, UK.

Electronic Supplementary Information (ESI) available: [details of any supplementary information available should be included here]. See DOI: 10.1039/x0xx00000x

motivation for this work was therefore to investigate whether similar trends holds for biomolecular-sensing BioFET experiments.

This review is divided into three main Sections. First, the operating principle of FET-sensors and relevant physiochemical properties of Streptavidin are introduced. Then relevant metrics for comparing device performance are critically reviewed, and finally, a quantitative analysis of streptavidin-sensing and pH-sensing literature is presented.

Operation of Field-Effect Sensors

FET-sensors are similar to Metal-Oxide-Semiconductor Field-effect Transistors (MOSFETs) wherein the gate is replaced by an electrolyte resulting in an oxide-electrolyte interface. An example setup is shown in (Figure 1). A voltage can be applied via a reference electrode in the liquid and operated similarly to the gate in a MOSFET, with gate voltage: V_g . For an n-channel device, an increasingly positive gate voltage will result in the formation of the conductive channel beneath the interface between the semiconductor and the gate insulator (oxide). In contrast, for a p-channel device, an increasingly negative gate voltage will result in the formation of the conductive channel. Whilst MOSFETs typically have highly doped contacts in order to form an inverted channel on application of a gate bias, in contrast, many FET-sensors do not have highly doped contacts and can operate in accumulation mode.

For a setup like that in Figure 1 featuring an insulating oxide layer, FET-sensor response is driven by changes in the electric field at the oxide surface due to analyte molecules binding to the surface. In the case of pH sensors, the FET-sensor is usually termed an Ion-Sensitive FET (IS-FET), and the surface is an oxide material in which pH-induced changes in the protonation state of the surface hydroxyl groups result in a change in the surface charge and therefore the surface potential. For sensing molecular analytes such as biomolecules, the surface is usually functionalised to provide receptor sites which are specific to the analyte and the device is usually termed a BioFET. The change in the interfacial electric field on binding of analyte causes a change in the concentration of charge carriers in the channel region of the device, with a corresponding measurable change in the source-drain conductivity.

Whilst Figure 1 shows a simple planar device geometry akin to a single-gate MOSFET, a plethora of device geometries have been developed such as nanogap²¹⁻²³, nanobelt^{24,25}, nanoribbon^{18,26-31} and nanowire^{15,28,32-36,37} structures. The application of additional lateral gates has been shown useful in tuning the carrier concentration of the device and pursuit of an optimal gate configuration is an active area of research³⁸⁻⁴⁰. There is also significant interest in the development of carbon-based devices^{14,41} which do not have an oxide layer such as graphene or carbon-nanotube devices. The advantage of these devices is stated to be potential sensitivity enhancement via (i) direct contact with analyte (ii) the size of the material being comparable to the size of the analyte⁴². It should be noted that the lack of a band-gap in graphene produces a limitation in the

ability of the transistor to transduce a change in surface potential to a change in current response⁴³.

The mechanism of operation of devices without an oxide layer, such as graphene and carbon nanotube devices, is expected to be different to those with an oxide layer due to the possibility of direct charge transfer from the analyte to the semiconducting nanotube layer^{44,45}. Due to the different mechanism of gating, these carbon-nanotube devices are not the focus of this review.

Under certain conditions discussed later, the transistor component has the capability of transducing a change in surface potential to an exponential change in current. While, in principle, changes in surface potential due to analyte binding can be measured directly without a transistor similarly to a conventional glass pH sensing electrode⁴⁶, this approach requires potentially large and expensive measurement equipment (high impedance amplifier). The FET-component facilitates miniaturisation of the device, providing smaller sample volumes and faster response times²⁰.

The Reference Electrode

Reference electrodes are used to provide a potential within the FET-sensor system to which other potentials can be referenced. Through the reference electrode, a gate voltage (V_g) can be applied in the sample and is sometimes referred to as a 'top-gate' voltage or 'liquid-gate' voltage in analogy to MOSFET operation. An ideal reference electrode ensures that the potential at the electrode-electrolyte interface is insensitive to changes in the electrolyte solution³². FET-sensors can be used to quantitatively measure binding of analyte as the response is a function of the electrolyte-oxide surface potential. The reference electrode provides a stable potential in the bulk electrolyte which is used to reference the measurement.

A stable reference potential requires a redox reaction in which there is constant thermodynamic activity of each participant in the reaction. In a conventional reference electrode, for example as used in electrochemistry or traditional glass-electrode pH sensors, this is achieved by placing a reference metal inside a compartment with a high concentration of salt solution connected to the analyte sample by a liquid junction which can only exchange ions⁴⁷. Miniaturisation of this system is problematic and results in reference electrodes with reduced lifetimes⁴⁷ and a common alternative in the field of FET-sensing is the pseudo-reference electrode in which a bare metal or chlorinated silver wire is used. Unlike conventional reference electrodes, the interfacial potential is not known *a priori*, but under controlled conditions can still maintain a stable potential.

Noble metal pseudo-reference electrodes such as Gold (Au) and Platinum (Pt) are sometimes used but cause issues with current instability and pH dependency³³. Although Pt-pseudo reference electrodes have been used in various streptavidin-sensing experiments^{34,48-50}, many research groups have reported that Pt pseudo-reference electrodes are unreliable and should not be used due to issues such as unstable potentials, transient noise and changes in electrical potential

due to non-specific binding of biomolecules ('bio-fouling')^{26,32,51,52}.

The most common pseudo-reference electrodes used in FET-sensors are silver-silver chloride (Ag/AgCl) electrodes which consist of a silver wire usually treated by either chemical or electrochemical chlorination⁵³. Rajan demonstrated experimentally that Ag/AgCl pseudo-reference electrodes are a suitable alternative to a conventional reference electrode⁵¹, with the proviso that, due to the strong interaction with chloride in the buffer, the chloride content of the buffer is kept constant throughout the sensing experiment. Both Rajan⁵¹ and Rim et al.³³ measured the open-circuit voltage between a Ag/AgCl pseudo-reference and conventional reference electrode to investigate bio-fouling and found the open-circuit voltage to be small, suggesting that pseudo-reference electrodes can be suitable for biosensing. For a more detailed review of pseudo-reference electrode validation experiments, see Supplementary Information Section 1.

The use of reference electrodes in FET sensors It is often stated that a reference electrode (with corresponding liquid-gate voltage, V_g) is required for a reproducible and stable signal from FET-sensors^{47,52,54,55}. Nonetheless, it is not uncommon for devices to be fabricated without any reference electrode in the liquid^{24,27,35,36,56} which can reduce the possibility of dielectric breakdown of the device under applied gate voltage (e.g. as described in the supplementary information of Stern et al.³⁵). Such devices often have a gate connected to the substrate (back-gate) which is either (a) at a constant gate voltage, usually chosen to optimise the transconductance of the device at that gate voltage, or (b) swept across a range of gate voltages in a similar way to which a liquid-gate might be operated. In case (a), the gate is essentially acting as a pseudo-reference electrode and this setup can be unreliable. In some cases the device can be unresponsive when operated via back-gate with no liquid top-gate^{26,51}.

The reference electrode setups used in the literature are broadly diverse; based on 37 publications identified in this review, 11% used Pt pseudo-reference electrodes, 19% used Ag/AgCl pseudo-reference electrodes, 11% used Ag/AgCl conventional reference electrodes, 21% did not publish their setup or it was ambiguously presented and 27% utilised only a back-gate. Of these setups, only Ag/AgCl pseudo-reference electrodes have consistently been proven to be capable of providing a reliable reference potential versus a conventional reference electrode.

Regions of Operation – Linear, Saturation and Subthreshold

The current flowing through a FET is controlled by the gate voltage, V_g and the drain voltage, V_{ds} . Depending on the particular choice of these two parameters, the device is said to be operating in one of three main regions: sub-threshold, linear and saturation. These regions are summarised graphically in Figure 2 and explained below.

The threshold voltage (V_T) is important in defining the region of operation and can qualitatively be described as the

minimum gate voltage (V_g) for which the device conducts a significant current and is therefore 'on'. More precisely, it describes the value of the gate voltage required to form an inverted channel, in which the induced carrier concentration in the inversion layer reaches the carrier concentration in the channel (bulk carrier concentration).⁵⁷ A detailed description of the threshold voltage and its significance to sensing is provided in Supplementary Information Section 2.

In a traditional Metal-Oxide-Semiconductor FET (MOSFET), when the gate voltage is low (i.e. $V_g < V_T$), the drain current (I) is referred to as the 'subthreshold current' and the device is operated in the 'subthreshold region'. This region is often used for FET-sensors because the response upon analyte addition can be enhanced^{28,37,51} with the drain current increasing exponentially rather than linearly dependent upon changes in the gate voltage⁵⁸. This is described by

$$I \propto e^{\frac{q(V_g - V_T)}{mk_b T}}, \quad (1)$$

where m is the empirical constant called the body-effect coefficient and q is the electronic charge. This expression is derived from MOSFET drift-diffusion equations shown in Supplementary Information Section 3.

If a larger gate voltage is used and the drain voltage is low (i.e. $V_g > mV_{ds} + V_T$, where m is an the empirical body-effect coefficient and $m \geq 1$ ⁵⁷) then the device is operating in the 'linear' region. If the drain current is high (i.e. $mV_{ds} + V_T > V_g$), then the saturation region is reached.

Device Characterisation

FET-sensors operate on the principle that binding of analyte to the sensor surface results in a change in surface potential ($\Delta\psi_s$) via electrostatic gating. This induces a change in the device threshold voltage, which can be measured via the transistor as an amplified signal in the form of a change in the drain current. By measuring the variation in drain current (I) as a function of the reference electrode potential, the shift in threshold voltage (ΔV_T) and the change in drain current (ΔI) can be measured. Either of these properties are termed device 'response' in this work. From these measurements, metrics important for characterising FET-sensors can be calculated. Commonly used metrics to characterise the sensor are the Subthreshold Slope (SS) for the subthreshold region of operation and the transconductance (g_m) for the linear region of operation. Common metrics for characterising sensor response to analyte are the Normalised Change in Current (I_{norm}) and the shift in threshold voltage (ΔV_T). These four metrics are illustrated in Figure 3 and are defined as follows.

The Subthreshold Slope (SS) is constant in the subthreshold region and therefore provides a straightforward quantification of device response in this region. The value of the SS is a measure of transistor quality in terms of its response to changes in the gate potential. It is defined as the change in gate voltage (V_g) needed to change the subthreshold current (I) by one decade⁵⁹ and is determined from measurements as the inverse

of the slope of the linear region on a ($\log_{10} I$) versus V_g graph at constant V_{ds} :

$$SS = \left. \frac{\partial V_g}{\partial (\log_{10} I)} \right|_{V_{ds}} \quad (2)$$

When V_{ds} is greater than a few $k_b T/q$ (where k_b is the Boltzmann constant and T is the temperature), the Subthreshold Slope is independent of V_{ds} because the current is diffusion-dominated⁵⁷. The Subthreshold Slope can be modulated by a back-gate voltage, $V_{g,back}$ ²⁹. The reciprocal of the Subthreshold Slope is also called the 'gate voltage swing' or 'subthreshold swing'⁵⁹.

The Subthreshold Slope can also be defined as:

$$SS \approx \frac{2.3mk_b T}{q} \approx \frac{2.3k_b T}{q} \left(1 + \frac{C_{dl}}{C_{ox}}\right), \quad (3)$$

where m is the body-effect coefficient, C_{dl} is the depletion-layer specific capacitance (per unit area) and C_{ox} is the specific capacitance of the oxide (per unit area)⁵⁷. Therefore, the Subthreshold Slope has a theoretical minimum value of approximately 59 mV/dec at room temperature. A lower value of the Subthreshold Slope corresponds to a larger change in current for a given change in the gate voltage, and therefore a Subthreshold Slope of 59 mV/dec corresponds to the upper limit for the current response of conventional FET-sensors⁴³. The subthreshold slope characterises the ability of the transistor to transduce a change in gate voltage to a change in current and therefore for both biosensors and pH sensors, the maximal change in change in current can only be obtained with an ideal (i.e. low value) Subthreshold Slope. This will be discussed later.

The transconductance, g_m , is constant in the linear region and is therefore particularly useful for describing the properties of the device in this region. Similar to the Subthreshold Slope, the transconductance measures the slope of the I versus V_g plot:

$$g_m = \left. \frac{\delta I}{\delta V_g} \right|_{V_{ds}} \quad (4)$$

The sensor response metrics are related to the effect of analyte binding producing a horizontal shift in the I - V_g curve⁴⁴, corresponding to a change in ΔV_T and a change in current, ΔI . The current-response (ΔI) can be used as the performance metric, in which case it is common practice to normalise the current (I_{norm}) as the change in current divided by the initial current.

Alternatively, ΔV_T can be used as a direct measure. Assuming an electrostatic gating mechanism, ΔV_T is equal to the change in surface potential, a direct indication that this parameter can be used for quantitative biosensing^{44,60}.

In some cases, however, the assumption of electrostatic gating is not valid. For example, if the metal contacts to the semiconductor are not well-passivated and therefore insufficiently protected from direct interaction with the analyte, analyte-induced changes to the metal-semiconductor work function produce a signal not originating from an electrostatic

gating mechanism^{20,44,61,62}. Another important example is if the reference electrode potential is modified by the analyte.

A detailed description of this can be found in the literature: Heller et al. describe how the I - V_g graph (transfer characteristics) can be used to diagnose the mechanism of FET response (e.g. electrostatic gating, work function change etc.)⁴⁴.

Streptavidin Biochemistry

Streptavidin is one of the most common model proteins used in biosensing studies⁶³ and its detection is often used as the initial proof-of-concept for new biosensor designs^{27,36,64}. The relevance of streptavidin is much broader; for example, Gupta et al. have shown that streptavidin has direct clinical relevance in capturing biotinylated interferon γ (MIG), which is a biomarker for several inflammatory and autoimmune disease states⁶⁵. Streptavidin is also commonly used in enzyme-linked immunosorbent assays (ELISA), a standard biochemical assay. As BioFETs can, in principle, detect the electric field generated by a single elementary charge^{66,67}, even small changes in the electrodynamic properties of streptavidin should be detectable, making an understanding of the charge properties of streptavidin important. Surprisingly, despite its common usage in BioFET experiments and most other biosensors⁶³, a rigorous description of its expected charge as a function of pH is not available. Furthermore, many publications do not report the commercial origin of their streptavidin samples under the assumption that it is not relevant to its charging-properties^{48,68-70}; in this section, based on analysis of published biochemical literature, this assumption is proposed to be false.

Streptavidin is a tetrameric protein composed of four identical subunits each with a high-affinity binding site for its ligand, biotin⁷¹. Strong chaotropic agents (6M urea) result in its dissociation into a dimeric form⁷². It is commonly used as a model protein in sensing studies for a variety of reasons. First, streptavidin has an extremely high affinity for biotin which can be quantified by its affinity constant (K_d) of approximately 10^{-15} M⁷³. Fast binding kinetics are evident from the association rate constant of greater than 10^7 M⁻¹s⁻¹.³⁴ A sensor surface can be given high streptavidin selectivity and affinity by functionalising it with biotin. Second, the ionic strength of the buffer affects the binding affinity and protein stability of many proteins but not streptavidin-biotin affinity⁷⁴. As discussed later, buffer dilution does still strongly affect sensor response due to screening effects. Third, it is well characterised, widely commercially available and there is an abundance of literature on chemical-functionalisation of biotin to sensor surfaces^{41,71,75}. Finally, the isoelectric point (pI) of streptavidin⁷⁶⁻⁸⁰ results in a near-neutral protein under physiological conditions, which reduces its propensity for non-specific binding. Despite these advantages, it should be noted that the unusually high affinity of streptavidin for biotin makes it unrepresentative of binding characteristics of most biomolecules.

The full sequence of streptavidin, as encoded by the native gene which is naturally expressed in the bacterium *Streptomyces avidinii*, is shown in Figure 4, with residues that are often charged shown as coloured and underlined. The blue

highlighted region is unlikely to be present in any commercial sample of streptavidin used for biosensing experiments as it is a signalling region that is removed *in vivo*⁸¹. The structure of streptavidin can vary between commercial preparations due to processing steps which result in artificial truncation of the protein, for example, in order to increase the protein solubility⁸². In 1990, Green stated that most, but not all, commercial samples of streptavidin were truncated⁷⁶. Since 1990, residues 15-159 of the native gene were used to express a recombinant form (i.e. artificially expressed in a non-natural bacterium) of streptavidin with increased solubility in the bacterium *Escherichia Coli*, and some modern commercial preparations of streptavidin are this recombinant form[†], adding further possibilities for variability between different commercial preparations.

In X-ray crystallography studies, Weber et al. reported that they were unable to crystallise non-truncated streptavidin, but successfully crystallised a truncated form of streptavidin⁷³, the sequence of which is highlighted in green in Figure 4 together with the full sequence for the protein. The pH-dependent charging properties of this structure were modelled, with a calculated charge of $-7.20e$ at pH 7.4 (Supplementary Information Section 4).

Examination of the sequence shows that, depending on where in the sequence streptavidin is truncated in different preparations, it is likely to differ in net charge by several elementary charge units. As high sensitivity sensors, BioFETs could in principle detect even small changes in the electrodynamic properties of streptavidin⁶⁶. A detailed analysis of streptavidin biochemistry literature (Supplementary Information Section 4) revealed that both the molecular weight and pI values can vary between different preparations with molecular weights in the range of between 53 and 66 kDa and pI values between 5 and 7.5⁷⁶⁻⁸⁰. This variation in pI and molecular weight is likely due to both variation in the biomolecular structure, and difficulty in obtaining accurate measurements of these properties. The resulting variability in electrodynamic properties (charge, kinetics etc.) will affect the reproducibility and comparability of experiments performed using different commercial preparations, and it is therefore recommended that the origin of the protein used in experiments is reported. This is not currently common practice; of the publications identified within this review (tabulated in Supplementary Information Section 5), 45% did not report the origin of their streptavidin sample.

In addition, surface-bound streptavidin has been measured with different properties to the free protein. The pI of surface-bound streptavidin has been measured using Surface Force Apparatus (SFA) and Atomic Force Microscopy which demonstrated a pI of 5.0 ± 0.5 ^{79,83}. Experimental determination of streptavidin pI is discussed further in Supplementary Information Section 4.

Other Biomolecules. This review focuses on streptavidin because it represents the most prevalent and comparable model protein system available at the time of writing, both in the general literature and that focussed on BioFET devices.

Another commonly used protein in BioFET studies is Avidin^{29,35,70}, which is related to streptavidin, has an affinity for biotin but has a higher pI and is therefore oppositely charged at the physiological pH. This protein however is a poor choice for comparative study for several reasons, firstly, electrophoresis reveals distinctive charge heterogeneity even in purified avidin and both compositional and structural heterogeneity due to its carbohydrate content⁸⁴, and secondly, its higher pI can result in higher non-specific binding due to a larger net-charge in physiological solutions⁸⁵.

Another biomolecule commonly used in BioFET experiments is prostate-specific antigen (PSA) due to biomedical applications as a prostate cancer biomarker, however the biomolecular capture step is more complex than streptavidin, requiring the use of a complex biomolecule such as an antibody or aptamer⁸⁶. The most well-studied biomolecule in BioFETs is undoubtedly nucleic acid-based systems such as DNA. However, as summarised in a review by Poghossian et al.⁸⁷, experiments are rarely performed using the same DNA-sequence or polynucleotide length, making their structural and electrical characteristics not easily comparable. Furthermore, in the DNA-sensing community there is high variability in experimental design, for example, the choice of buffer composition⁸⁷.

Buffer Solution

The buffer solution maintains the pH and the stability of the biomolecule, the system and the measurements. Its composition, the concentration and ratios of ions in solution, can have a significant effect on the bio-sensitivity of the sensor. Even in absence of biomolecules, ions in the buffer can modulate the surface chemistry or be selectively adsorbed to the surface, generating a detectable response. Accurate reporting of the composition of this solution is therefore essential to any biosensor experiment.

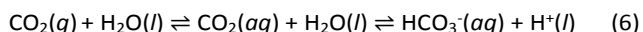
Buffering Capacity. An important property of the buffer for biosensing experiments is the 'buffering capacity', which quantifies the capability of the buffer to maintain a constant pH, where the pH is defined as the negative logarithm of the hydrogen ion activity:

$$\text{pH} = -\log_{10}(a_{\text{H}^+}) \quad (5)$$

Phosphate buffer is often used for biosensing experiments; a convention is to define 10 mM ionic strength phosphate buffer as 1X $\text{NaP}_i = \text{Na}_2\text{HPO}_4$ (8.1 mM) and NaH_2PO_4 (1.9 mM). The most common buffer for protein sensing is Phosphate-Buffered Saline, PBS, which is composed of 1X NaP_i mixed with 138 mM NaCl and 2.7 mM KCl⁷⁴. The ionic strength of 1X PBS is 162.7 mM⁷⁴. Some confusion can arise where authors use the acronym PBS for 'Phosphate Buffered Solution', as it becomes ambiguous whether they are reporting NaP_i or PBS⁶⁹. This distinction is often critical since, as discussed in Supplementary Information Section 1, when a Ag/AgCl pseudo-reference

electrode is used, then the chloride content of the buffer can significantly change the reference potential⁵¹.

The $\times X$ dilution notation is often used in this field due to the relevance of ionic strength and because dilution is often required for larger signals, as discussed later. Dilution can introduce a variety of issues, for example, at high dilutions (e.g. 0.01X PBS) the buffering capacity of the solution is reduced meaning that the system can become highly sensitive to small pH changes. For example, even the experimentalist breathing near the sample can result in elevated $\text{CO}_2(g)$ dissolved into the sample and being detected⁸⁸ as per:



This introduces a potential source of noise to the measurement.

A related issue arises upon addition of large amounts of biomolecule to a solution. Adsorption or release of protons to/from the surface of the biomolecules can affect the pH of the bulk solution. Lloret et al. measured the bulk change in pH using a pH microelectrode in response to addition of streptavidin and found that for 1 μM streptavidin in 0.01X PBS (a common dilution), there was a change of 0.5 pH units⁷⁴. In contrast, at 1X PBS the shift in pH was negligible due to the high buffering capacity. The significance of this cannot be understated; for a typical PBS concentration of 0.01X, and a typical SiO_2 surface in the pH 5 to 9 region ($\Delta V_{T,pH} \approx 30$ mV/pH response), this would correspond to a non-specific response of $\Delta V_T = 15$ mV due to bulk pH change; which is of the same order of magnitude as most measured streptavidin signals.

A simple experimental control is to ensure that only low concentrations of analyte are used. This is more relevant to medical diagnostic applications in which biomolecules often must be detected at low-concentrations from blood samples.

Proper controls can reduce variability due to non-specific binding and lack of buffering capacity. Fully washing the surface with the analyte buffer (without analyte) can remove signal due to non-specifically bound streptavidin, however washing is not solely sufficient for specific biomolecule detection. One strategy to isolate non-specific binding response is to perform an experiment in which streptavidin pre-saturated with biotin is added and then the device is washed; in the case of specific-binding, this should show no significant response⁴⁸. To demonstrate that the signal is due to specific biomolecule binding, Stern et al. utilised a cleavable-biotin molecule and confirmed that the device response could be restored to baseline by biotin-cleavage³⁵. Lloret et al. suggested tailoring the buffer to have the highest possible buffering capacity while being both suitable for the biomolecule and having an ionic strength low enough to allow analyte sensing, for example, NaP, rather than PBS.

Ionic Strength and the Debye length. The ionic strength of the buffer can affect biosensing response in two ways: via modification of the surface chemistry or modification of the screening length.

The Debye length is the characteristic length scale for charge screening of electrolytes under the Debye-Hückel model⁸⁹. This

concept can be useful when considering BioFET operation on large biomolecules which may contain charges located several Debye lengths away from the surface. In high ionic strength solutions, the Debye length is short so that distant charges would be screened and have no significant effect on the surface potential. Dilution reduces the ionic strength of the solution and extends the Debye length; however, this can cause ancillary issues such as a reduction in buffering capacity and instability of the biomolecule in solution⁹⁰, or reduced affinity of the biomolecule-target interaction, although the latter is not the case for streptavidin⁷⁴. For PBS dilutions of 1X, 0.1X and 0.01X, the calculated Debye lengths are 0.76 nm, 2.41 nm and 7.61 nm respectively⁷⁴. Stern et al. demonstrated a significant BioFET response for binding of streptavidin in solution to biotin on the sensor at 0.01X PBS, but no significant response at 1X PBS. Approximating streptavidin as ~ 5 nm from the surface⁷³, they found that this result agrees with the Debye-Hückel model.⁹¹

Whilst the concept of Debye screening is useful in explaining reduced response in high ionic strength systems, caution must be taken in its use. For example, Bergveld⁹² used the Debye-Hückel model of the electrical double layer to argue that charged biomolecules cannot be detected at high ionic strengths, having written:

'The resulting double layer, with a thickness of the Debye length, is of the order of 1 nm thick in moderate electrolyte concentrations. Beyond this distance no external electric field exists. Hence the idea that a layer of charged molecules at the surface of an ISFET modulates the electric field in the gate oxide should definitely be forgotten' (emphasis added) - Bergveld (1996)⁹².

In the Debye-Hückel model, the Debye length is ~ 1 nm at ~ 160 mM ionic strength and yet streptavidin has been detected at this ionic strength by various authors^{65,69,93} and similar observations can be found for other biomolecules^{65,94}.

Even under the assumption that the Debye-Hückel model describes the system accurately, there are several misapprehensions which should be highlighted. First, the Debye length is not a hard cut-off beyond which no electrostatic effect is felt because the screened Coulombic interactions reach to infinity. This can be seen from the expressions from the Debye-Hückel model at an electrode-electrolyte interface:

$$\psi_r = \psi_0 e^{-\frac{r}{\lambda_D}} \quad \text{and} \quad E_r = \frac{\psi_0}{\lambda_D} e^{-\frac{r}{\lambda_D}}, \quad (7)$$

where ψ_r is the potential as a function of radial distance r , and λ_D is the Debye length. Second, it is also assumed that molecules are rigid and bound in a fixed orientation, whereas in reality they are flexible and dynamic and therefore some orientation of the analyte can bring the molecular charges closer to the surface than other orientations⁹⁵.

A further consideration is that the surface chemistry itself can change at different ionic strengths, resulting in alteration of the sensor response. For example, the FET-sensor of Tarasov et al. showed a shift in threshold voltage of 59 mV for every 10-fold increase in KCl concentration⁹⁶. They attributed this effect to pH independent selective adsorption of anions. Similarly, a non-linear FET-sensor response to increasing NaCl concentration was measured by Maekawa et al⁹⁷. This empirical

observation has also been observed in molecular dynamics simulation studies^{97,98}.

The Electronic Device and Signal Drift

Physical and structural characteristics of the transistor device, particularly the choice of semiconducting material, can affect both the amplification ability of the transistor and its performance in terms of drift. Silicon is commonly used as the semiconductor material rather than more exotic materials, as its ubiquitous presence in the semiconductor industry means that fabrication is simple, well-understood and low cost. Silicon-based FET sensors can, however, suffer from long-term unidirectional drift in signal. Various mechanisms for this action have been proposed⁹⁹ yet this remains an important research question within the field as it is a key factor limiting commercialisation efforts. ~~There is evidence to suggest that it is related to ions from the aqueous solution diffusing into the insulating material and~~ and/or, in the case of Si₃N₄ films, via aqueous hydration of the surface to SiO₂ ~~or an oxynitride~~^{99–103}. While SiO₂ surfaces are rapidly hydrated, Si₃N₄ surfaces and other common oxide materials such as Al₂O₃ and Ta₂O₅ are known to be more resistant to hydration¹⁰¹ and show reduced drift rates at pH 7¹⁰⁴.

Given the timescale of the drift often observed in SiO₂ surfaces (hours) device noise or drift could be due to ions from the aqueous solution diffusing into the insulating material^{101,105} which would show a corresponding change in the threshold voltage of the device¹⁰¹. As an alternative material ~~to SiO₂~~ which is impermeable to ions⁹⁵, AlGaIn/GaN-based FETs have been demonstrated with significantly reduced drift in physiological buffers and various groups have successfully utilised AlGaIn/GaN-based devices for streptavidin sensing^{48,49,65,106,107}.

Understanding and modelling drift characteristics of FET-sensors remains a vital challenge in the field. As an illustration of this, there remains no physical model capable of accurate quantitative modelling of experimental signal drift for gas-based FET-sensors¹⁰⁸.

Recent Developments

For successful commercialisation of BioFETs in biomedical applications, operation in high ionic strength environments remains a key engineering challenge. An alternative mode-of-operation for sensing FETs has been proposed, first by Schasfoort et al.^{109,110} and recently demonstrated for detection of poly-L-lysine¹⁷. This mode relies on making a sudden change in ionic strength change ('ion-step') and measuring the initial non-equilibrium response before the system fully equilibrates. More recently, Krivitsky et al. detected biomarkers from untreated blood samples using a similar strategy in which the transient response from specific-binding is compared to a non-specifically bound control¹¹¹. By measuring the transient response of the system, biomolecules can potentially be detected in higher ionic strength buffers than conventional 'equilibrium' sensing experiments. This also potentially offers

better sensitivity to the analyte and reduced sensitivity to the background drift in the drain current.

Other methods have shown promise at circumventing Debye screening limitations. For example, FET nanogap-devices operate on a different mechanism to conventional BioFETs, where the dielectric constant of the gate is modified by analyte binding and the device is operated after drying^{21,22,112}. Another example for conventional FET-sensors is that the surface layer could be modified with a biomolecule-permeable polymer layer which is proposed to operate by extending the effective distance over which charges are screened within the layer¹¹³. A final example of particular interest is the use of frequency-mode detection^{15,45,114–117}, where the current response is measured in the frequency domain instead of the time-domain (details can be found in Supplementary Information 6).

The lack of wide-spread adoption of alternative operating methods may be due to: complexity, with the additional required steps required making them less commercially appealing; a lack of awareness in a rapidly changing field; or lack of reproducibility. Given the variety of strategies which have shown some efficacy at circumventing the limitations arising from charge screening, it is likely that this will successfully be surmounted in a commercial device.

Device Performance Metrics

Given the lack of maturity of FET-sensor technology, it is understandable that this field have not yet converged upon a set of standards, both in terms of well-defined nomenclature or usable engineering parameters. Such nomenclature and parameters are required to rigorously compare the performance of BioFET sensors, particularly the metrics involved in the detection and quantification of analytes.

IUPAC Definitions

IUPAC defines 'sensitivity' as a metric of the specific response as a function of the analyte concentration. More specifically, it is defined by IUPAC as 'the slope of the calibration curve'. IUPAC defines the calibration curve as:

'The functional (not statistical) relationship for the chemical measurement process, relating the expected value of the observed (gross) signal or response variable to the analyte amount. The corresponding graphical display for a single analyte is referred to as the calibration curve'.¹¹⁸

The IUPAC definition of sensitivity is not a measure of the ability to detect the minimal amount of an analyte, and therefore a second relevant metric is the Limit of Detection which IUPAC defines as the smallest measure that can be reasonably detected for a given analytical procedure, and is expressed as a concentration or quantity. More specifically:

'The limit of detection, expressed as the concentration, c_L , or the quantity, q_L , is derived from the smallest measure, x_L , that can be detected with reasonable certainty for a given analytical procedure. The value of x_L is given by the equation $x_L = \bar{x}_{bi} - ks_{bi}$, where \bar{x}_{bi} is the mean of the blank measures, s_{bi} is the standard deviation of the blank measures, and k is a numerical factor chosen according to the confidence level desired'.¹¹⁸

Analysis of Sensitivity

The IUPAC definition of sensitivity incorporates two elements: the measurement of a specific response, and its dependence upon analyte concentration. Some BioFET publications have quantified sensor performance using a definition of 'sensitivity' which differs from the IUPAC definition. For example, some authors refer to the absolute change in current (ΔI) or, more frequently, the change in current divided by the initial current is referred to as the 'sensitivity'. To avoid confusion and for comparison, a clear set of nomenclature is defined in this section for use in this review.

The symbol I_{norm} is used to refer to the Normalised Change in Current, which is defined as:

$$I_{\text{norm}} = \frac{I_f - I_0}{I_0} = \frac{\Delta I}{I_0}, \quad (8)$$

where I_f and I_0 are final and initial values of the current, respectively.

Some publications simply refer to the absolute measured change in current from the device (ΔI) as the metric however, this results in a large device-to-device variation. The Normalised Change in Current has become common practise as it reduces this variation¹¹⁹. The reason for this reduction in device-to-device ratio is that the absolute current is directly dependent upon geometric parameters and threshold voltage of the device, whereas the Normalised Change in Current is only subject to device-to-device variation from differences in the device threshold voltage¹¹⁹. Further, the change in current (ΔI) can either be positive or negative and consequently the Normalised Change in Current, I_{norm} , also has an associated sign. Some authors have reported the Normalised Change in Current without this sign which makes the polarity of the measured change ambiguous⁴⁸.

Response in the Subthreshold Region. A key factor when operating in the subthreshold region is the exponential relationship between threshold voltage and drain current (Equation 1). As a result, a +10 mV change and a -10 mV change in threshold voltage do not produce an equal and opposite Normalised Change in Current.

This can be explored using the MOSFET drift-diffusion equations and the shift in threshold voltage (due to analyte binding) can be related to the Normalised Change in Current using the following equation^{18,43}:

$$\Delta V_T = SS(\log_{10}(I_{\text{norm}} + 1)). \quad (9)$$

This equation can be used to calculate the expected magnitude of I_{norm} for a given analyte. For example, considering the case of an ideal n-channel transistor with a Subthreshold Slope of 59 mV/dec and an analyte that induces a change in threshold voltage of 10 mV, the calculated I_{norm} is approximately -33%. For the equivalent analyte and a p-channel device, the calculated change in I_{norm} is approximately +50%.

This important distinction between a negative I_{norm} and a positive I_{norm} can be emphasised as a qualitative difference; A

current which decreases is 'bounded' by zero and therefore has a maximum possible value of -100%, whereas an current which increases has no mathematical upper limit for I_{norm} . In this paper, this is referred to as 'unbounded' to indicate that is always positive and can reach large positive values. In the subthreshold region, a direct comparison between an unbounded signal from one device (negative molecule on an n-channel semiconductor) and the bounded signal of another (i.e. with a p-channel device) is uninformative. This is particularly relevant for ambipolar devices (e.g. the devices of Nam et al.¹²⁰); ambipolar devices can operate in either an n-branch or a p-branch depending on the choice of gate voltage, requiring a metric which can compare the response of the unlike branches.

In order to compare the signal between devices with different channel types, the change in current can be normalised by the current obtained either before the response (I_0) or after the response (I_f), whichever is lower. These lowest and highest values are referred to as I_{low} and I_{high} respectively. This results in an I_{norm} which is always positive and 'unbounded' with no mathematical upper limit. This 'unbounded' metric is herein referred to as I_{norm}^+ or the 'unbounded Normalised Change in Current':

$$I_{\text{norm}}^+ = \frac{I_{\text{high}} - I_{\text{low}}}{I_{\text{low}}} = \frac{|\Delta I|}{I_{\text{low}}} \quad (10)$$

The differences between the unbounded and bounded I_{norm} are illustrated schematically in Figure 5. For consistency with our previous quantitative analysis of the literature performed for pH sensing¹⁸, I_{norm}^+ was used in this analysis. As an example, for streptavidin (negatively charged analyte at pH 7.4) on an n-channel device, the drain current would decrease and therefore I_{low} would be the drain current after addition of streptavidin and I_{high} high before addition. Alternatively, it would be possible to compare the 'bounded' change in current, where the current is normalised by the higher of the current (I_{norm}^-) before or after binding.

Concentration Dependence. Normalised Change in Current is a function of the amount of bound analyte as well as the ability of the sensor to amplify response. This can be problematic from the perspective of biosensor design, because if an experiment is performed on a very poor sensor (i.e. low ability to transduce chemical binding into measurable signal) with a high concentration of bound analyte, then the resulting I_{norm} value can be the same as that measured by an experiment on a superior sensor with a low concentration of bound analyte. The response per 10-fold increase in concentration of analyte is a more useful figure-of-merit for biosensors and is similar to the IUPAC definition of sensitivity. In BioFET literature, the Normalised Change in Current is often calculated based on the change in drain current after the introduction of an arbitrary concentration of analyte. In contrast, in pH sensing literature, it is often defined over a single pH unit (i.e. per 10-fold increase in concentration of analyte).

Other than as a figure-of-merit, there are important scientific reasons for the measurement of the response as a

function of analyte concentration. The affinity (i.e. equilibrium dissociation constant, K_d) of an analyte binding to a sensor can be estimated by fitting the concentration-dependent response data to an appropriate binding model³⁴. Further, the concentration at which the response saturates can be used to estimate the density of bound molecules^{27,121}. Note that at concentrations much greater than the K_d of the binding reaction, sensor saturation occurs, along with increased levels of non-specific binding¹²².

Performance metrics have also been discussed by Rajan et al.^{28,51}, who highlighted a few examples from the literature of concentration-response curves for BioFETs over different analytes and stressed the importance of considering, not only the IUPAC sensitivity, but also the Signal-to-Noise Ratio (SNR). At this time, unfortunately, most BioFET data is reported without noise analysis or sufficient repeats to obtain an estimate of the statistical uncertainty of measurements, and so quantitative estimation of this SNR or IUPAC limit of Detection is rare. Given these limitations, the analysis presented in this analysis uses the Normalised Change in Current per 10-fold increase in analyte concentration (e.g. % per unit pH or % per 10-fold increase in streptavidin concentration) as a performance metric to compare sensing results between different experiments. This metric will be referred to as 'Sensitivity' due to its similarity to the IUPAC definition and will be discussed in more detail later and in Supplementary Information 7.3.

Sensitivity Limits. Sensor response is improved with a larger shift in surface potential, and therefore knowledge of the upper and lower limits for the surface potential shift is an important aspect of sensor design. In pH sensing, a maximum shift in surface potential of approximately 59 mV/pH is observed, in good agreement with the theoretical prediction given by the Nernst model of equilibrium potentials of ions across semi-permeable membranes¹²³. While it is reasonable to consider that a similar limit would apply to biomolecular surface-binding experiments (~59 mV per 10-fold increase in streptavidin concentration at room temperature), there are significant differences between proton equilibria and macromolecular biomolecule binding equilibria, which implies that the Nernst model is not applicable to protein binding. As a result, the existence of such a macromolecular 'surface-potential response limit' remains an open research question. Shoorideh and Chui hypothesised that no such limit for biomolecule binding exists because the high affinity of biomolecular-ligand binding would result in the extent of binding being independent of the surface potential, in contrast to proton-binding where the binding is exponentially related to the potential of the surface^{124,125}.

The largest shift in threshold voltage for a pH sensor can be calculated based on the Nernstian response of 59 mV/pH. The steepest Subthreshold Slope for a classical transistor is approximately 59 mV/dec⁴³. From Equation 9, the largest Normalised Change in Current is obtained when the Subthreshold Slope is steepest and the shift in threshold voltage is largest, resulting in an upper theoretical Sensitivity limit of 900%/pH. Lee et al. used additional circuitry intended to

amplify the FET-signal beyond this value but did not provide quantitative evidence to support that it had improved the signal-to-noise ratio or limit of detection¹²⁶.

Relationship between Surface Potential and Current Response

I_{norm} is a measure of the amplification of the current response. By contrast, ΔV_T is a measurement of the changes in the electrostatic potential at the surface and therefore can be used both to provide quantitative detection of analyte and also to suppress device-to-device variation^{119,127}. The change in threshold voltage due to analyte binding can either be measured directly from the shift in the $I-V_g$ curve, or calculated using MOSFET drift-diffusion equations (Supplementary Information Section 3 and 8). The analytical relationship between current change and the change in threshold voltage is dependent upon the region of operation of the FET as follows.

For FET-sensors operated in the subthreshold region, this relationship is given by Equation 9^{18,37,43} and has a logarithmic dependence on I_{norm} . In the subthreshold region, the transconductance is variable as a function of gate voltage and therefore cannot be treated as a constant.

For FET-sensors operated in the linear regime, ΔV_T can be extracted experimentally by simply dividing the current-response data (ΔI) by the device transconductance, g_m ^{28,60,119,128}:

$$\Delta V_T = \frac{\Delta I}{g_m} = (V_g - V_{T,0}) I_{\text{norm}}. \quad (11)$$

This expression is only valid if the analyte does not change the operating regime of the device⁶⁰ and providing that g_m is the same before and after binding³⁴ (i.e. electrostatic gating mechanism of FET operation⁴⁴). Alternatively, the threshold voltage prior to analyte addition, $V_{T,0}$ and I_{norm} can be used to calculate the shift in threshold voltage⁵¹. Derivation of these equations can be found in Supplementary Information Section 8.

Signal-to-Noise Ratio Enhancement

This section presents common methodologies to obtain, optimise and understand the Signal-to-Noise Ratio (SNR) properties of FET-sensors as a figure-of-merit for biosensors.

Optimal Region of Operation. There are a number of noise sources such as semiconductor-device resistance, type of measurement equipment, electrolyte-interface chemistry and electrolyte-reference electrode chemistry. When comparing devices with similar noise levels and operating in the subthreshold region, an improved Subthreshold Slope is expected to improve the Limit-of-Detection. From Equation 9, where for a minimum detectable Normalised Change in Current, a device with smaller Subthreshold Slope results in a smaller required shift in surface potential, and therefore a lower required concentration of analyte for detection.⁴³

An important relevant question is: what gate voltage and region of operation is best for SNR and IUPAC limit of detection, given that the noise varies between devices and as a function of

gate voltage? For the current response, the SNR is defined as the ratio of the change in current ΔI to the noise in the measurement (δi) response.

Empirically, there are various methods for determining the noise component. Given the low-frequency noise is of interest for biosensing, and that the most common noise source of FET-transistors is of the form $1/f$ (flicker noise), a common approach^{45,51,107,129,130} utilises the following expression:

$$(\delta i)^2 = \int_{f_1}^{f_2} \frac{S_I(f=1 \text{ Hz})}{f} df = \ln\left(\frac{f_2}{f_1}\right) S_I(f=1 \text{ Hz}) \quad (12)$$

where $S_I(f=1 \text{ Hz})$ is the drain current noise power spectral density at 1 Hz and the integral is between the largest and smallest frequencies sampled. Given that $\ln(f_2/f_1)$ is only weakly dependent upon the choice of bandwidth in most sensing experiments, this can be neglected to give a simplified calculated metric for SNR:

$$\text{SNR}_{\text{metric}} = \frac{\Delta I}{\delta i} = \frac{\Delta I}{\sqrt{S_I(f=1 \text{ Hz})}} \quad (13)$$

Sometimes ΔI is converted into the voltage regime using $\Delta I = g_m \Delta V_T$, however care must be taken with this equality as transconductance is constant only in the linear region (Equation 11) or can only be accurately treated as such for small changes in threshold voltage.

There is experimental evidence from a number of authors demonstrating that the subthreshold region has better Signal to Noise Ratio. Operating in the subthreshold regime improved the SNR for the BioFET device of Gao et al. who measured prostate-specific antigen (PSA) binding and found the optimum I_{norm} agreed well with the maximum in SNR, but did not explain how SNR was calculated³⁷. They explained their result giving resistive noise as the dominant noise source, which is proportional to carrier density and therefore greatly decreased in the subthreshold region. Tarasov et al., who performed noise analysis of an ion-sensitive FET both in air and at pH 7 and defined the SNR as the reciprocal of the equivalent noise power of the threshold voltage, also demonstrated improved SNR in the subthreshold region³⁰. Heller et al. performed charged-molecule sensing and salt concentration-change sensing experiments and remarked that for their device, measurement at peak transconductance provided poorer SNR than measurement in the subthreshold region⁴⁴.

Contradictory evidence also exists. Rajan et al.¹³⁰ performed noise analysis upon various systems with different buffers and showed peak SNR in the linear region close to the point of peak transconductance. The disagreement with other devices in the literature was explained as the device having a different regime of mobility fluctuation noise¹³¹. Rajan also investigated the SNR due to binding of streptavidin to biotin functionalised surfaces, over a range of gate voltages⁵¹. A high concentration of D-biotin in the bulk could displace surface-biotin-bound streptavidin so that the same sensor could be reused at various gate voltages. Increased SNR was then observed as the gate voltage was moved from the subthreshold region into the linear region⁵¹. In summary, the evidence suggests that although operation in the

subthreshold region often improves SNR, its ability to improve SNR may be system dependent.

A related question is therefore what region of operation is optimal for sensor Sensitivity (e.g. I_{norm} per pH). In the linear region (Equation 11), I_{norm} increases as the gate voltage V_g approaches the threshold voltage V_T , i.e. as the subthreshold region is approached. I_{norm} is always optimised in the Subthreshold Region. Once the subthreshold region is reached, Equation 11 becomes invalid and an alternative expression (Equation 9) for the Normalised Change in Current is recovered, which is a function of the Subthreshold Slope and is independent of gate voltage. To demonstrate that these theoretical relations hold experimentally, Figure 6 shows the results from the BioFET streptavidin binding experiment of Wen et al.⁴⁸ with all the relevant parameters plotted (I_{norm} , ΔI , I and g_m).

In summary, in the subthreshold region Sensitivity is optimised as a result of the large Normalised Change in Current, I_{norm} , which occurs when the initial drain current, I_0 , is small, however in this region of operation, the noise of the low drain current may become larger than the signal and therefore SNR or IUPAC limit of detection are not necessarily optimal.

Effect of Electrolyte and Surface Chemistry. An important question with regards to the SNR is whether it is an intrinsic property of the device or whether the electrolyte solution has a significant effect. Rajan et al. defined the SNR as the transconductance (g_m) divided by the square root of the current noise power density (S_I) and measured this in pH sensing experiments^{129,130}. Focusing on the low-frequency range (around 1 Hz), they found that variation in ionic strength produced a negligible change in the SNR and concluded that the SNR an intrinsic property of the device¹³⁰. They showed that the SNR can be maximised by tuning the gate voltages¹³⁰, and increasing sensor area¹²⁹. They also stated that their device had a surface functionalised with (3-Aminopropyl)triethoxysilane (APTES) and demonstrated improved SNR and reduced current noise power compared with a bare SiO_2 surface¹²⁹, hypothesising that the APTES lowered the effective density of trapped charges at the oxide-electrolyte interface.

Lu et al. investigated low frequency noise (~ 4 Hz) in devices with a bare SiO_2 surface but saw that the noise was ionic strength dependent. From the paper, a 0.001 M PBS system showed a current noise power density which was 70% noisier than in 0.1 M PBS buffer, while the current noise power density showed only small pH dependence¹³². Their results were partly rationalised with a number fluctuation-dominated current noise model but the authors acknowledged that the fluctuations cannot be fully explained in terms of modulation of the charge trapping probability with changes in ionic strength.

Back-gated Operation. The carrier concentration within the device and its distribution between gates can be tuned by applying a fixed back-gate voltage¹³³, although a back-gate is not inherently required in a FET-sensor. This back-gate bias can be applied –to optimise the transconductance/Subthreshold Slope with respect to a sweep of the ‘top-gate’ reference

~~electrode in the liquid, (for liquid-exposed top-gate voltage sweep, like that shown in Figure 3),~~ resulting in a ~~consequent~~ improvement of the Normalised Change in Current^{29,38,134–137}. This process is sometimes described as double-gated FET (DG-FET) operation^{129,138}. Importantly, modifying $V_{g,back}$ does not change the intrinsic properties of the electrolyte interface and therefore the top-gate shift in threshold voltage $\Delta V_{T,top}$ is constant as a function of sweeping $V_{g,back}$ ²⁹. Alternatively, the back-gate voltage can be swept with the top-gate held fixed, thus resulting in a plot of I versus $V_{g,back}$ similar to Figure 3 but in which the dependent variable is $V_{g,back}$ instead of $V_{g,top}$. From this plot, $\Delta V_{T,back}$ can be measured, which is related to $\Delta V_{T,top}$ but amplified.

The phenomenon was described by Go et al. as the result of capacitive coupling within the system¹³⁴. The coupling amplified a change in top-gate voltage ($\Delta V_{T,top}$) which consequently results in an amplified shift in bottom-gate voltage ($\Delta V_{T,back}$) which depends upon the capacitance of the liquid-exposed top-gate dielectric (C_{top}), the back-gate dielectric (C_{back}) and a factor (α_{SN}) with a value between 0 and 1 depending on the extent of coupling due to the choice of biasing conditions¹³⁴:

$$\Delta V_{T,back} = \Delta V_{T,top} \frac{C_{top}}{C_{back}} \alpha_{SN}. \quad (14)$$

Pud et al. explain the physical origin of this phenomenon as due to the applied back-gate voltage shifting the conducting channel from the oxide-semiconductor interface to the bulk semiconductor where less scattering occurs and a higher mobility is attained¹⁶. Further research is required in this field for the development of a general theory of back-gated operation. The $\Delta V_{T,back}$ threshold voltage shift amplification strategy has been utilised for biosensing, such as the work of Duan et al.³⁴ and Jayant et al.^{139–141}.

While there is no doubt that double-gated FET operation can amplify the measured voltage shift, an important question that remains is whether it can provide an improved SNR. Go et al. concluded that double-gated FET operation can only improve the SNR if the noise from the measurement equipment sets the lower limit of performance¹³⁴. In the double-gated FET operation of Pud et al., noise spectroscopy revealed an improved SNR¹⁶. Regardless, the use of a back-gate voltage offers the advantage of reducing the requirements for external circuitry to amplify the signal. Go et al. derived a quantitative model of double-gated FET operation which can explain the results of some systems; in their model the response is a result of capacitive coupling between the back-gate and the top-gate oxides, and under certain gate voltage conditions, the semiconductor body capacitance¹³⁴.

Device Geometry. Finally, a great deal of literature is focused upon the investigation of new device-geometries aimed at improving Sensitivity, SNR or Limit of Detection. The commonly stated argument that increased surface area-to-volume ratio increases the Normalised Change in Current^{27,35,142,143} is the rationalisation for much of the focus in publications on creating devices with nanoscale dimensions. This argument is still

subject to debate, with some authors suggesting that nanoscale dimensions offer increased response via a different mechanism^{125,144} or that the argument is not generally applicable to all structures¹⁴⁴. Operating in the linear region, the SNR was calculated and measured to increase with the square root of the device area for constant device thickness¹²⁹. This assumes that the entire surface contributes uniformly to the signal, and therefore is expected to apply to pH sensing and to biosensing experiments in which there is sufficient analyte to cover the surface receptors uniformly¹²⁹.

It has been demonstrated both experimentally^{27,35,142} and theoretically^{142,143} that increasing surface area-to-volume ratios increases Normalised Change in Current. Operating in the subthreshold region, the improvement is attributed to the Subthreshold Slope improvement (i.e. decreased value) which results from the improved ratio of oxide capacitance to depletion-layer capacitance (Equation 3). There is no evidence that nanowire or nanoribbon geometries can achieve a better Subthreshold Slope than the ideal value of 59 mV/dec through their superior surface area-volume ratio. Particularly, it is worth noting that scaling in channel length results in degradation of the Subthreshold Slope due to the Short Channel Effect (SCE)¹³⁸. Planar devices are capable of providing comparable Sensitivity to nanoscale devices given that planar devices can be made with a Subthreshold Slope of ~80 mV/dec for bulk¹³⁸, or ~63 mV/dec for fully-depleted silicon-on-insulator (SOI) transistor or ~~and~~ double-gated SOI transistor devices¹⁴⁵. Nanocrystalline MoS₂ thin films (with a HfO₂ oxide layer) are also shown capable of obtaining a near ideal subthreshold slope of ~60 mV/dec⁴³. However, increased surface area-to-volume ratios provide other advantages such as improved biomolecule binding kinetics and therefore reduced response time^{146,147}. A reduced response time would improve the effective Limit of Detection within practical time-constraints (e.g. several minutes)^{146,147}. For planar devices at very low concentrations of biomolecular analyte (femtomolar), the time-to-equilibration of the response may be impractically long; if measurements are taken pre-equilibration of the biomolecular surface binding reaction of the surface, the 'effective' Sensitivity between two devices, after the same fixed time, would be higher for the device with shorter response time. Furthermore, nanoscale geometries offer increased potential for miniaturisation.

Quantitative Analysis

Methods

This analysis compares FET-sensor results for pH-sensing with streptavidin-binding to oxide-APTES-(or the methoxysilane equivalent, APTMS)-biotin-functionalised surfaces. Where available, the parameters such as the Subthreshold Slope and Normalised Change in Current were directly extracted from the streptavidin literature, and where this was not reported explicitly it was extracted manually from I - V_g graphs.

As discussed, when comparing Normalised Change in Current between devices of different types (i.e. p- or n- channel device), normalisation simply using the 'initial' drain current,

prior to analyte addition, is insufficient. The change in drain current was normalised by the lower drain current to give the 'unbounded' Normalised Change in Current, I_{norm}^+ , using Equation 10. As this was used consistently through this analysis, the symbol I_{norm} will be used to refer to the unbounded change in the rest of this review. As an example, for streptavidin on an n-channel device, the drain current is expected to decrease after addition of streptavidin and therefore I_{low} will be the drain current after addition of streptavidin and I_{high} before addition. This is consistent with our previous quantitative analysis of the literature for pH sensing¹⁸.

For publications which present streptavidin-sensing data as a function of concentration of streptavidin, it is possible to calculate the 'Normalised Change in Current for a 10-fold increase in streptavidin concentration', and equivalently for pH sensing, the response due to a change of 1 pH unit was used (pH is related to the proton concentration, Equation 5). Assuming a linear relationship between a 10-fold change in analyte concentration (e.g. a pH unit for pH sensing) and a 10-fold change in current, then I_{norm} per 10-fold increase in analyte concentration is expected to be a constant. Therefore, for a set of n 10-fold changes in analyte concentration, the largest current after n 10-fold changes in concentration (I_n) can be calculated from the lowest current (I_0) and the Normalised Change in Current (I_{norm}):

$$I_n = I_0(I_{\text{norm}} + 1)^n. \quad (15)$$

For an n-channel device with a negatively charged biomolecular analyte, I_n and I_0 correspond to the lowest and highest concentration of analyte, respectively. Rearranging for I_{norm} gives an expression for the representative Normalised Change in Current per 10-fold increase in analyte concentration:

$$\text{Sensitivity} = \left(\frac{I_n}{I_0}\right)^{\frac{1}{n}} - 1, \quad (16)$$

and will be referred to as 'Sensitivity'. In this expression, I values for which the current response has saturated are excluded. The Sensitivity can also be calculated from a set of $I_{\text{norm},i}$ values (Supplementary Information Section 7.3). The Sensitivity facilitates comparison of current response between experiments performed at different analyte concentrations and is similar to the IUPAC definition of sensitivity (discussed previously).

Note that not all published data are presented both unambiguously and with completeness. As a result, sometimes paper-specific assumptions had to be made in order to complete this analysis. These assumptions are explained in detail in Supplementary Information Section 7.4.

Surface Binding Reactions

Equilibrium Response. For quantitative biosensing experiments, the relationship between biomolecule concentration and response is required. Assuming electrostatic gating, the shift in the threshold voltage (ΔV_T) is related to the shift in surface potential at the oxide-electrolyte interface ($\Delta\psi_0$) (discussed in Supplementary Information Section 2). The

precise relationship between the addition of biomolecular charge and the change in surface potential remains one of the most important modelling problems in this field^{20,139–141,148–157}, however an appealing model, due to its simplicity, is to approximate the oxide-electrolyte interface as a parallel plate capacitor (Helmholtz–Perrin Theory)¹⁵⁸. The change in charge on the surfaces of the capacitor, ΔQ , with capacitance C_0 can give the voltage shift simply as:

$$\Delta\psi_0 \approx \Delta V_T = \frac{\Delta Q}{C_0}. \quad (17)$$

From this simple model it can be seen that a concentration-dependent response with increased biomolecule binding to the surface is expected, a response demonstrated by many authors for streptavidin sensing^{25,27,31,35,48,50,107,120,159–165}.

The simplest model for biomolecule-binding reactions, is the first-order Langmuir model of surface-reactions (details in Supplementary Information Section 10). In this model the surface reaction of analyte (A) to the surface sites (S) is treated simply:



The resulting equilibrium constant, $K_d = [AS]/([A][S])$, bears many similarities to the well-known pK_a for the case of proton-binding, as illustrated in Figure 8. Solving the rate equation for the above system and finding the steady-state solution analytically, results in the Langmuir equation, also shown in Figure 8.

The equilibrium coverage, modelled by the Langmuir equation, is related to device response. As a result, the dynamic range of the sensor (i.e. the concentration range of analyte upon which it operates) can be seen to be fundamentally limited by K_d . At bulk concentrations $[A]_0 \gg K_d$, the sensor is expected to be saturated. For systems in which there is a low K_d , such as streptavidin-biotin binding, based on the Langmuir equation, the high affinity means that a large proportion of the total number of sites $[S]_{\text{max}}$ are expected to be occupied (i.e. $[AS]/[S]_{\text{max}} \sim 100\%$) even at low concentrations of bulk analyte. For surface-bound systems, there is evidence to suggest the K_d may be smaller than the solution measured K_d ¹⁶⁶.

If a finite volume of analyte is used and the ligand has a high affinity, then the effects of finite numbers of sites can become important as the bulk concentration of ligand can be depleted by reactions to the surface¹⁶⁷. Rajan utilised numerical simulation to demonstrate the consequences of ligand-depletion on the equilibrium coverage ($[AS]/[S]_{\text{max}}$) and showed that in low K_d , small volume systems (i.e. low number of molecules available for binding), the equilibrium coverage is significantly lower than that predicted by the Langmuir isotherm, and with increasing numbers of receptors (e.g. with increased receptor-functionalised sensor area) this effect is exacerbated⁵¹. For example, if a 50 μL solution contains 1 fM solution of biomolecule, then 301 streptavidin molecules are in solution. Assuming one biomolecule binds to one receptor, and a K_d of 1 fM, then the equilibrium coverage predicted by the

Langmuir equation is 50%. For a large sensor (well functionalised sensor, $\gg 301$ receptors) an equilibrium coverage of much less than 50% would be expected because all the biomolecule would have depleted from solution and bound to the many available receptors.

The lower Limit of Detection of the sensor is restricted to single-molecule binding; the critical concentration at which only one target molecule binds the sensor at equilibrium c_{min} , to a sensor of area A with density of receptors $[S]_{max}$ ¹⁶⁸:

$$c_{min} = \frac{K_d}{[S]_{max}A} \quad (19)$$

A simple strategy for estimating the maximum density of bound molecules can be demonstrated. When measuring the response as a function of the analyte concentration, a concentration at which response is saturated (c_{max}) occurs. Assuming binding occurs specifically to receptors at the surface (i.e. no multilayers) then the saturation concentration corresponds to the upper limit of the density of specifically-bound biomolecule²⁷. To demonstrate this analysis, various examples from streptavidin-sensing publications are used.

From the work of Elfström et al.²⁷, given a sample volume, V , of 200 μL solution and concentration, c_{max} , of 0.5 nM, the total number of molecules in the solution ($= c_{max}V$) can be obtained. Assuming all molecules bind to the surface (valid given $K_d \ll$ streptavidin concentration at the surface) and that they bind homogeneously, then the bound density, ρ , will simply be $c_{max}V$ divided by the functionalised area, A , exposed to analyte (10 mm^2):

$$\rho_{Elfström} = \frac{c_{max}V}{A} = 0.015 \text{ molecules nm}^{-2}.$$

This can be compared with the maximum streptavidin density, ρ_{max} , theoretically possible for streptavidin, assuming each molecule occupies $\sim 25 \text{ nm}^2$.⁷³

$$\rho_{max} = 0.04 \text{ molecules nm}^{-2}.$$

This comparison suggests that the surface-bound density for the device of Elfström et al. is close to ideal. In contrast, if this is compared to Duan et al.³⁴ who showed a c_{max} of 2 pM, taking into account the different sensor areas and amount of streptavidin[†], then a significantly lower surface coverage is calculated:

$$\rho_{Duan} = 0.000072 \text{ molecules nm}^{-2}$$

This lower surface site density may well be explained by low levels of functionalisation of the surface. These calculations are useful as they provide an estimate of surface site density, i.e. functionalisation success rate, and ultimately dictates an upper limit for response. They can also inform experimental design when choosing sensible concentration ranges to perform experiments under. If a sensor has low functionalisation density, then it may also have a poor response time (a long time for proteins to diffuse to the binding sites).

Won Hee Lee et al.³¹ and Wen et al.⁴⁸ did not report the volume of analyte solution utilised, making this analysis impossible. However, using the data from Stern et al., a similar calculation can be performed. Their nanowire-based FETs were selectively functionalised, in principle creating a device with very low active surface area^{35,169}. Fluorescence imaging confirmed that there was selective binding of streptavidin¹⁶⁹. Given the surface area and sample volume of their device[†], the calculated saturation concentration c_{max} should be approximately 20-200 fM, however the measured signal increased up to 1 nM. A possible explanation for this disagreement would be that the high concentration response is due to longer-range interactions from streptavidin not directly bound to the nanowires (e.g. multilayer coverage) or that despite the selective-functionalisation, there is sufficient non-specifically bound streptavidin on the device that the effective concentration at the surface of the nanowire is much lower than the initial bulk concentration.

If there were a linear relationship between analyte-binding and receptor-concentration, then it would be possible to extract the density of biotin on the surface from this simple analysis of sensor response as a function of analyte concentration. However, experiments have shown a non-linear relationship between biotin concentration at the surface and sensor response. Duan et al. showed a response saturation for polyelectrolyte films containing 30% biotin¹⁷⁰ which agrees well with the Surface Plasmon Resonance (SPR) experiments of Jung et al. who showed saturation with an alkylthiolate monolayer containing 34% biotin¹⁷¹. The non-linearity in the concentration-dependence is likely a combination of steric constraints of the protein and the fact that streptavidin has four binding sites. Jung et al. observed that streptavidin binds to one site for low concentrations of biotin (0.34% biotin), two sites for peak saturation (approximately 30% biotin), and that for high biotin content (>40% biotin) the biotin became less available within the monolayer due to reorientation ordering, resulting in less binding to streptavidin¹⁷¹. If this result is transferable to other chemical functionalisation systems, it counter-intuitively suggests that extremely high-density biotin functionalisation would be detrimental to Sensitivity.

Kinetic Response. For a system that is reaction-limited (reaction rate is slower than diffusion to the sensor surface from the bulk) the response is expected to increase with time but diminish exponentially. Streptavidin-biotin is unusual in that it has an exceptionally high affinity which results in diffusion-limited kinetics (the reaction is faster than diffusion to the surface). For this an initially linear response is expected, as has been shown by Duan et al. for streptavidin-biotin binding³⁴ (Supplementary Information Section 10.2).

For ultra-low concentrations of biomolecules, a lower value of the Subthreshold Slope can decrease the response time for a given signal change. The reason for this is that for a given change in signal, a lower Subthreshold Slope value requires a smaller change in surface potential. Assuming that the bound biomolecule concentration is proportional to surface potential

change, a smaller number of bound molecules is required and therefore the time-to-detection is reduced^{43,172}.

The transport of analyte to the surface of the sensor is important for setting the time-to-response and therefore the effective detection limit within a given time-frame. For example, using simple analytical arguments to describe the diffusive flux, detection of 1 fM biomolecular analyte using a 30 nm radius nanowire is expected to take an average detection time on the order of hours, compared to orders of magnitude longer using planar devices^{146,147}. In contrast to biomolecular sensing, pH sensing provides fast response times as the diffusion constant for H⁺ is orders of magnitude higher due to Grotthuss transport, in which H⁺ transport along hydrogen bonded networks^{173,174}. The theoretical detection time for an individual proton is non-trivial to calculate due to the complexity introduced by acid-base equilibria and Grotthuss transport, which cannot be described by simple Brownian motion¹⁷⁵. In summary, for BioFET design the limitations imposed by the mass transport, binding kinetics and geometry choices should be considered when designing for optimal response^{51,146,168,176}.

Non-specific Response. The concentration of biomolecular analyte available to bind to the surface may be lower than that expected based on the initially added bulk concentration due to binding to non-sensitive regions of the device, an issue which is often caused by non-specific binding but can also occur if biomolecular receptors have been functionalised on solvent-exposed regions of the device away from the sensor (e.g. if the passivation layer shown in Figure 1 was functionalised). This is particularly problematic for nanoscale dimension devices in which the sensing region of the device can have a small surface area relative to the total exposed surface area²⁵.

Streptavidin Sensing Data

In this section, current-response data for the detection of streptavidin is presented for devices with oxide-APTES-biotin surface functionalisation and streptavidin sensing.

Linear Region. Measurements in this region of operation have been reported which show detection of streptavidin at the oxide-APTES-biotin interface^{24,34,43,48,120}. Data from these publications is tabulated in Supplementary Information Sections 5 and 9. Three publications contained data with response as a function of streptavidin concentration, giving a Sensitivity of 72%¹⁶¹, 63%¹²⁰ and 0.5%⁴⁸. As discussed previously, the linear region is not expected to optimise I_{norm} or Sensitivity and therefore measurements in this region are not the focus of this review.

Subthreshold Region. Many publications only provide the change in response due to addition of an arbitrarily determined concentration of streptavidin. As a result, only the Normalised Change in Current can be used for comparison and the Sensitivity cannot be calculated for such papers. In this section, I_{norm} from across the streptavidin-sensing literature is

extracted and presented with the corresponding shift in threshold voltage for devices operated in the subthreshold region. A tabulated summary of papers identified can also be found in Supplementary Information Section 5.

FET-sensor data was obtained from nine publications in which streptavidin binding to oxide-APTES-biotin coated surfaces was measured in the subthreshold region, and is shown in Figure 7. The Normalised Change in Current, I_{norm} , is plotted against the device Subthreshold Slope. The data was obtained from experiments which were not all performed at the same concentration of streptavidin and at more than one ionic strength. Where experiments were performed at several concentrations of streptavidin, or at differing ionic strength, this is indicated in the figure. For experiments performed at a higher concentration of streptavidin, there is a higher density of bound analyte (until the sensor surface is saturated) and a corresponding increase in I_{norm} .

If the Normalised Change in Current was measured between several different concentrations, the Normalised Change in Current for each is shown on the graph and the relative concentration used is indicated via the size of the marker symbol. No clear relationship between the Normalised Change in Current and Subthreshold Slope was observed. High ionic strength can reduce response and therefore increasing ionic strength is indicated in Figure 7 with a thicker marker outline.

Each solid curve shown in Figure 7 shows the calculated shift in threshold voltage for a given Subthreshold Slope and I_{norm} (from Equation 9), and therefore it can be seen that most measurements correspond to a shift in the threshold voltage, ΔV_T , of between 5 mV and 165 mV.

Data analysis of responses in Streptavidin and pH Sensing

Introduction. The optimal response of a pH sensor can be estimated using Equation 9, which provides the relationship between changes in surface potential and FET current response in the subthreshold region. This equation shows that Sensitivity is expected to be a function of the transistor Subthreshold Slope and shift in threshold voltage.

Oxide materials demonstrate a surface potential variation which is approximately linear as a function of pH (over a narrow range of pH values), which can therefore be represented as a single number, for example, a SiO₂ surface typically has a pH-induced surface potential change of 33 ± 6 mV/pH¹⁸. For this system, a maximum pH Sensitivity of between 190% to 360% is calculated assuming an optimal Subthreshold Slope of 59 mV/dec (ideal at room temperature). This is useful for the design of pH sensors as it indicates that optimal Sensitivity in the subthreshold region can be obtained by choosing a dielectric with high pH Sensitivity (e.g. HfO₂ rather than SiO₂) and engineering a good transistor (low Subthreshold Slope). An important research question is whether simple device-design strategies like these can also be developed for biosensing, which is a primary motivation for this analysis.

The precise relationship between pH Sensitivity and biomolecular Sensitivity remains an active area of research^{68,74,141}. Shalev et al. provided evidence to suggest that

biomolecular sensing may be a result of biomolecules altering the chemical equilibria of titratable groups on the surface, and therefore for some systems pH-Sensitivity and biomolecular-Sensitivity are expected to be related⁶⁸. In this analysis pH-sensing and biomolecular-sensing Sensitivity have been considered separately.

The analysis in this section focuses upon pH-sensing and streptavidin/biotin interactions on FET devices operating in the subthreshold region.

Results. Where sufficient data was available, Sensitivity was calculated for the previously presented streptavidin-sensing data^{25,27,31,48,69,107} and the results are plotted against Subthreshold Slope in Figure 9. In our previous work¹⁸, we published a collation of pH sensing data^{18,37,43,177–184}, using a metric equivalent to Sensitivity, and this data is also included in Figure 9.

As shown in Figure 9a, the Sensitivity values ranged between 3% and 84% per 10 fold increase in Streptavidin, whereas the pH-sensing Sensitivity varied between 1% and 600% per pH. Therefore, on the basis of available streptavidin-sensing data, a value for Sensitivity in streptavidin-sensing comparable to optimal pH sensing has not been obtained. The pH-sensing results are consistent with a response of 33 mV/pH for SiO₂ systems and 59 mV/pH for HfO₂ systems. In order to better visualise the calculated shift in threshold voltage, the Subthreshold Slope of each data point and corresponding Sensitivity value was inserted into Equation 9 to obtain the calculated shift in threshold voltage per 10-fold increase in analyte concentration for that measurement. This was then used to plot Figure 9b. In this figure, isocontours calculated using Equation 9 are drawn from red to blue for values of the Sensitivity increasing in 1% increments in the range 1-150%. From Figure 9b, again it can be seen that the pH sensing data showed a shift in threshold voltage which is generally consistent for a particular oxide material (~33 mV/pH for SiO₂ with one anomaly, ~59 mV/pH for HfO₂ with one anomaly), in contrast to the streptavidin-sensing data (oxide-APTES-biotin surface chemistry) which showed no clear trend in threshold voltage shift.

Discussion. A large degree of the variability in response illustrated in Figure 7 is due to the variety of concentrations of analyte used between different experiments. In order to account for this variability, the Sensitivity was calculated and presented in Figure 9a. From the streptavidin-sensing data, the maximum Sensitivity (up to 84%³¹) was lower than the maximum observed in pH sensing data (up to 600%⁴³). For some devices^{27,31,48,107}, the Sensitivity for biomolecular analyte was similar to that expected from a pH sensor with the same Subthreshold Slope, however for the devices of Liu et al.²⁵ and Buitrago et al.⁶⁹, a significantly lower Sensitivity than pH sensing results was obtained, despite the low Subthreshold Slopes (112 mV/dec and 95 mV/dec respectively). This can be explained as a consequence of the fact that these biosensing experiments are not obtaining both the high shift in surface potential and low Subthreshold Slope that is required for a high

Sensitivity (shown more clearly in Figure 9b). It should be noted that the low Sensitivity of 2% seen in the study of Buitrago et al.⁶⁹ may be simply a consequence of the response not being measured at equilibrium, as in Buitrago it was stated that analyte was 'immediately washed away by PBS'¹⁸⁵. The high Sensitivity of Won Hee Lee et al.³¹ of 84% may be unreliable given a key claim of the conference paper is that Subthreshold Slope is changing with increased analyte concentration and this is not clearly demonstrated in the paper (as discussed in Supplementary Information Section 7.4).

Regarding the calculated shift in threshold voltage per 10-fold increase in analyte concentration (Figure 9b), for pH sensing, the results showed a shift in threshold voltage per pH which was consistent with the material of the oxide, as previously observed in the literature¹⁸. Specifically, despite the fact that the pH sensing results are from disparate literature sources, they show highly consistent threshold voltage shifts of ~33 mV/pH (SiO₂) and ~59 mV/pH (HfO₂). Most SiO₂ systems show a pH response of approximately 33 mV/pH^{18,37,177,178}, with some reports demonstrating a higher value of 43 mV/pH¹⁸⁶, 46 mV/pH⁹⁷ and 42-50 mV/pH¹⁷⁹ which may be due to different surface preparation procedures. Other oxides demonstrate higher values, such as Ta₂O₅ at 52 mV/pH¹⁸⁰ and HfO₂ at approximately 59 mV/pH^{43,181–184}. One pH sensing result⁴³ in Figure 9b can be seen to exceed the Nernst limit (59 mV/pH) with a calculated threshold voltage of 66 mV/pH. This result is likely due to small error in the extraction of the Subthreshold Slope: in the high Sensitivity, low Subthreshold Slope region of the plot, the effect of small errors in Subthreshold Slope is high. As an example, for this measurement, an error of only 8 mV/dec in the extraction of the Subthreshold Slope would place this result within the Nernst limit.

The physical origin for these material-consistent surface potential shifts can be explained in terms of surface complexation models, also known as site binding models, which were first introduced by Yates et al.¹⁸⁷ and later refined by Healy et al.¹⁸⁸. In these models, an increased density of hydroxyl groups on the surface corresponds to an increase in surface potential shift per unit pH^{123,186}. This theory is supported by experimental work which has shown that blocking hydroxyl groups on the surface with organic functionality can reduce the surface potential shift per pH^{123,189,190}.

At the lower limit, Figure 9b shows that most oxide surfaces demonstrate surface potential shifts as a function of pH which are above approximately 25 mV/pH. As this value is a shift per 10-fold increase in analyte ($\text{pH} = -\log([\text{H}^+])$), this can be contrasted to streptavidin sensing experiments, which showed both: (a) a greater variation in possible shifts in threshold voltage per 10-fold increase in streptavidin concentration and, (b) the possibility of very low shifts of less than 10 mV (Liu et al.²⁵ and Buitrago et al.⁶⁹). If a device has a shift in threshold voltage per 10-fold increase in streptavidin concentration that is < 10 mV, it can be seen in Figure 9b that it is theoretically impossible to obtain a Sensitivity value greater than approximately 50%. This form of analysis can be used to provide information for improved BioFET design; it suggests that if a

device shows a low threshold voltage shift per 10-fold increase in analyte, then design focus should be put upon enhancing the change in surface potential by optimising the surface chemistry. Below we hypothesise an explanation for this contrast in pH and biosensing data, and posit that such considerations are needed in order to design BioFETs which are as sensitive to analyte as the already commercially-successful (pH) ion-sensitive FETs.

Comparison of Streptavidin and pH sensors

There are many potential factors which could explain the observed differences in the threshold voltage shifts between pH-sensing and biosensing experiments. Several of these factors relate to the surface and its chemistry. Figure 10 shows a schematic which attempts to summarise possible differences in the surface chemistry, and therefore measured surface potential shifts, between pH and biosensing experiments. This section explores each of these factors in relation to the operation of a FET sensor system, highlighting the important implications for the understanding and design of such a sensor for biomolecules. Each section heading is labelled corresponding to the labels within Figure 10.

Receptor Density (i). Given the ability of Surface Complexation Models to explain the observed shifts in threshold voltage for pH sensing data, it is plausible a similar mechanism can explain much of the variation in biosensing data. In pH sensing, the density of analyte receptors is described by the density of hydroxyl groups at the oxide surface, whereas for streptavidin-biotin biosensing the density of analyte receptors is the density of biotin available at the sensor surface. Using analogous arguments to those used in Surface Complexation Models, an intuitive hypothesis is that the shift in threshold voltage per 10-fold increase in analyte concentration is primarily limited by the density of receptors (and therefore bound-analyte) on the surface.

In order to investigate this, analysis of the concentration-dependent response curve was performed to infer the density of bound-biomolecule. As an example, the device of Elfström et al. in Figure 9b demonstrated a surface potential shift of 52 mV per 10-fold increase in streptavidin, which is large compared to the majority of other streptavidin-sensing measurements and pH-sensing measurements. The density of streptavidin molecules upon the surface of the device of Elfström et al. was calculated to be near to the ideal density for close-packed streptavidin. It should be noted that their device was operated without a reference electrode at fixed back-gate voltage, which is generally believed to be required for a well-defined signal. This supports the hypothesis that the biosensing shift in threshold voltage per 10-fold increase in streptavidin concentration is largely determined by the density of surface receptors. Optimising the density of receptors and the sensor surface area is ~~therefore~~ important in improving the device response¹²⁹.

Response Times – Non-Equilibrium Response (ii). In addition to receptor density as one factor that may affect the threshold

voltage shift, there are many other potential factors which could explain the observed differences between pH-sensing and biosensing experiments. The shift in threshold voltage per 10-fold increase in analyte concentration for biosensing may be lower than that for a 10-fold increase in H^+ concentration in pH sensing simply because the biomolecular response measured may not be fully time-equilibrated. As discussed, transport of the biomolecule to the surface and the subsequent reaction can take a long time to equilibrate compared to the equilibration of the acid-base reactions relevant to pH sensing. The limitations imposed by mass transport, binding kinetics and device-geometry choices must be considered when designing for optimal biomolecular-sensing response^{51,168,176}.

Non-specific Binding (iii). The concentration of biomolecular analyte available to bind to the surface may be lower than that expected based on the initially added bulk concentration due to binding to non-sensitive binding. If the concentration of analyte at the surface is overestimated because of non-specific binding, the effective threshold voltage shift per 10-fold increase in analyte is reduced.

Biomolecular Charge (iv). As discussed in the streptavidin sequence analysis and literature review, variation between different experiments may occur due to different commercial preparations of the same biomolecule having different electrodynamic properties.

Biomolecular Orientation (v). In principle, the biomolecular orientation can affect the response. Molecules such as antibodies are known to be oriented in a statistical manner rather than unidirectional as often indicated in schematics.^{95,149}

Buffering Capacity (vi). The buffering capacity of the solution, is important in determining the stability, reliability and accuracy of the measurement. Low buffering capacities can result in additional noise from ambient fluctuations in pH, for example, due to reactions with carbon dioxide in the air changing the acidity of the solution.

As previously discussed, signal change being directly proportional to bound-analyte is a weaker assumption for biomolecule sensing, because the bulk pH of the solution can be modified by analyte and detected by the sensor⁷⁴. The practice of using minimal buffering capacity and high biomolecule concentration (added in a single aliquot) is not uncommon^{25,43,65,106,119,191} leading to a solution which is not buffered adequately. Low concentrations of analyte are closer to the reality of applications in medical diagnostics in which biomolecules are often only present at low concentrations within blood samples. Alternatively a solution should be used which has the same buffering capacity as PBS at a lower ionic strength, for example, using just the Sodium Phosphate component of the PBS buffer.⁷⁴

Ionic Strength (vii). As discussed, variability in ionic strength between experiments is expected to result in variability in the

response due to changes in the extent of screening of the biomolecular charges.

Nanoscale Device Geometry (viii). The analysis in Figure 9a shows that using a simple planar (macroscopic) device, Wen et al.⁴⁸ and Won Hee Lee et al.³¹ achieved higher Sensitivity than the nanobelt arrays of Liu et al.²⁵ and Cheng et al.²⁴ or the nanowires of Elfström et al.¹²¹. This shows that even simple planar geometries can obtain high Sensitivity for biomolecule detection compared to more complex nanoscale geometries. As introduced previously, whilst nanoscale devices can offer improved Subthreshold Slope compared to conventional devices, nanoscale dimensions are not required to obtain a near-ideal Subthreshold Slope for a device. For pH sensing, a consequence of this is that planar devices can provide similar Sensitivity to nanoscale devices, and that their response accurately determined by the choice of oxide (i.e. shift in threshold voltage per pH) and the Subthreshold Slope¹⁸. In contrast, for biomolecular sensing, the shift in threshold voltage per 10-fold increase in analyte is not primarily determined by the choice of oxide material, and can instead be explained as due to the aforementioned factors e.g. the receptor density.

Summary and Future Outlook

Biosensor design is a highly interdisciplinary field. Understandably, this has led to a diverse range of experimental designs and varying goals, resulting in many publications focusing on some aspects of sensor characterisation in more detail than others. It is important going forwards that clear standards be developed and used for the purpose of developing reliable sensors with reproducible and translatable characteristics.

Reporting the drain current as a function of top-gate voltage is encouraged, as this provides information on the quality of the transistor, but also can be used to extract information regarding the change in surface potential at the sensor surface-electrolyte interface. This information can be used to quantitatively compare sensor capability.

At this stage in FET-sensor research, the focus is predominantly upon Sensitivity-enhancement. As the field moves toward commercial applications, it will become increasingly important to provide controls which evidence specificity as well as Sensitivity. In order to maximise Sensitivity, many BioFET experiments are performed at high concentration of biomolecules with low buffering capacity solution (diluted buffer), potentially resulting in a significant non-specific response due to biomolecule-induced changes in the bulk pH of the solution.

Metrics of reporting device performance have been discussed. The Normalised Change in Current (I_{norm}) is currently almost ubiquitously used performance metric in the field and is useful for characterising the current response as it often reduces device-to-device variation compared to the absolute change in current. The Normalised Change in Current is optimised in the subthreshold region, which is not necessarily the region of optimal SNR. The region of optimal SNR has been

shown to be device dependent, with reports of optimum SNR both near to the region of maximum transconductance (which is usually in the linear region) and in the subthreshold region. An improved figure-of-merit that has been proposed in the literature is the SNR or IUPAC limit-of-detection, which involve identifying the noise levels in the signal. The importance of reporting the polarity of the Normalised Change in Current should be emphasised, as the absolute value can lead to ambiguity in interpreting experimental results.

Reference electrodes are crucial for consistent and reliable sensing results, however, the difficulty in reference electrode miniaturisation has led to common usage of pseudo-reference electrodes in their place. Several publications suggest that Pt-based pseudo-reference electrodes are unsuitable for reliable sensing. In contrast, Ag/AgCl pseudo-reference electrodes have the potential to be a viable alternative to conventional reference electrodes. Using a back-gate as the pseudo-reference electrode without a top-gate liquid (pseudo-) reference electrode has been reported to provide unreliable results. The use of a top-gate liquid electrode together with an optimised back-gate electrode voltage which modifies the carrier concentration profile within the device can improve the Subthreshold Slope. By using a fixed top-gate liquid electrode voltage and sweeping the back-gate voltage, a measurement can be performed resulting in an amplified back-gate threshold voltage shift, however in this setup any SNR enhancement is expected only when the measurement equipment sets the lower limit of performance.

Streptavidin biochemistry was reviewed, and it was shown that there is a significant amount of variability for structural and electrical properties of streptavidin between different preparations of the biomolecule. An analysis of the sequence was presented which highlights that different commercial preparations are likely to have different structures, and as even small changes in electrodynamic properties of a biomolecule are in principle detectable by a BioFET, it is recommended that authors report the commercial origin of their biomolecule for reproducibility.

For pH sensing, it is known that the Sensitivity can be increased by optimising the transistor design such as to have a low value of the Subthreshold Slope and by choosing an oxide material which has a large shift in surface threshold voltage per pH e.g. HfO₂. In contrast to Sensitivity in pH sensing, the analysis of the literature presented in this review revealed that streptavidin-sensing Sensitivity showed no clear dependence on Subthreshold Slope. This observation can be attributed to streptavidin-sensing demonstrating a much greater variation in the threshold voltage shift per 10-fold increase in analyte concentration between devices, even when devices shared the same oxide material. This study shows that the pH sensor design-strategy in which focus is upon Subthreshold Slope optimisation and oxide material choice *does not* directly transfer to biosensing, because, for example, a poorly functionalised biosensor surface is expected to always have negligible Sensitivity regardless of the choice of oxide. This has addressed one of the original motivations of this work to investigate whether optimisation strategies that had been

employed for pH sensors would be directly transferable to optimisation of biomolecular sensing. The analysis presented suggests that Subthreshold Slope improvement is not likely to be as beneficial for biosensor optimisation as it is for pH sensing because the limiting factor for Sensitivity is often the surface chemistry. In conclusion, the quantitative analysis presented here suggests that in order to optimise FET-sensor Sensitivity, the device should be operated in the subthreshold region. Device design optimisation should focus upon the simultaneous optimisation of both the Subthreshold Slope of the device and the electrolyte-oxide surface chemistry. For example, even using an ideal classical transistor (optimal Subthreshold Slope of approximately 59 mV/dec), if the surface is poorly functionalised with analyte receptors it will have a low Sensitivity.

The variability in the shift in threshold voltage per 10-fold increase in analyte concentration for biosensing responses was greater than that found for pH sensing responses. This higher variability can be explained by a variety of factors. pH models predict the most important factor in influencing this shift is the density of analyte-receptor (e.g. hydroxyl groups) at the surface, and therefore this could be an important factor determining the variability in biomolecular response. Further, the effects of ionic strength and buffering capacity in biosensing are much more pronounced than for pH sensing due to the biomolecule distance from the surface, and due to the ability of the biomolecule to change the pH of the buffer. Additional variability in biosensing threshold voltage shift per 10-fold increase in analyte concentration can originate from loss of biomolecule due to non-specific binding. This is particularly problematic for nanoscale dimension devices in which the biosensitive regions of the device can have a small surface area relative to the total exposed surface area. As discussed, a fundamental source of variability can originate from the biomolecule itself.

By measuring the response-curve as a function of analyte concentration, researchers are provided with important information for device design: the saturation point of the curve can indicate the density of bound analyte, the response per 10-fold increase in analyte concentration can provide a figure-of-merit for the device and by fitting the curve to an appropriate binding model, the binding affinity of the analyte to its receptor can be estimated. Simple calculations can be used to estimate the density of bound analyte based on the concentration at which the sensor response saturates, and both this value and measurement of the shift in threshold voltage per 10-fold increase in analyte concentration can be useful in determining whether Sensitivity enhancement efforts are limited by surface chemistry or transistor performance.

Devices even of simple (microscopic) planar geometry were shown capable of obtaining comparable Sensitivity to more elaborate nanodevice geometries (such as nanowires), suggesting nanoscale device design is not a requisite for high biomolecular Sensitivity. Due to process control constraints, the subthreshold slope is limited to ~ 63 mV/dec, with a theoretical lower limit of 59 mV/dec at room temperature. Therefore, it is expected that no further Sensitivity gain is obtained by further

scaling of device geometry for equilibrated (with respect to the analyte binding reactions) pH sensing and biomolecular sensing experiments. This contradicts the commonly accepted claim that a high surface-to-volume ratio is a requisite for high biomolecular Sensitivity. Nanoscale device geometries are however expected to offer improved response times for biomolecular detection, and therefore improve both the effective Limit of Detection given practical time-constraints for a sensing experiment.

State of the art devices operate by modulating the resistance of the semiconductor (with an upper limit of 59 mV of change in gate voltage to a decade of current change) by modulating the local carrier concentration in the semiconductor. For the published nanowire sensors, the nanowire dimensions are commonly around 100 nm in width and therefore far larger than typical biomolecule dimensions, resulting in the same sensing mechanism between nanowires and conventional sheet channel. Looking to the future of the field, an interesting possibility would be the fabrication of a novel BioFET (with semiconductor insulated from electrolyte with a dielectric, i.e. operated by field-effect mechanism) such that the width scale of the device is comparable to typical biomolecular dimensions (on the order of ~ 1 -2 nm width and thickness). In contrast to present devices, the channel of such a device could be completely inverted by individual biomolecules, which can result in different Sensitivity and SNR characteristics. A competing challenge for such a design would be the challenge of fine dimensional control which is beyond the limit of top-down fabrication technology as well as the local variation in discrete dopant sites (discrete dopant fluctuations) within the semiconductor, which results in significant variation in device-to-device Sensitivity and, in turn, presents a significant issue for reliable detection of single molecules without the use of additional circuitry¹⁴³.

Many of the current limitations which have been presented are similar to those that have been encountered for other emerging biosensing technologies. The current 'gold standard' for label-free biosensing is Surface Plasmon Resonance (SPR) biosensors. In a highly extensive review published in 2005, Rich and Myszka analysed 1113 articles (103 reviews, 1010 papers) and discussed common issues within the Surface Plasmon Resonance biosensor literature such as: authors only considering high concentrations of analyte, response being normalised inappropriately or the data was reported in insufficient detail¹⁹². Surface chemistry optimisation has played an important part of Surface Plasmon Resonance biosensor development¹⁹³. In principle, BioFET devices have the potential to surpass Surface Plasmon Resonance biosensors due to their potential for low-cost fabrication, ability to detect low-mass analyte and the elimination of the requirement for additional optical equipment (which can be high cost and low throughput).

As highlighted in this review, current advances in the field of BioFET research are being obstructed by the lack of consensus upon which quantitative metrics (i.e. figure-of-merit) should be used to compare devices, with the result that most published studies can only be compared qualitatively. Despite this, BioFET research is a rapidly advancing field in which novel device design

and operation methodologies are consistently being developed. Owing to the widespread capability for integration of this type of technology with the portable electronics used in Point of Care analysis and wearable technology, the potential for BioFET sensors to revolutionise approaches to biosensing in healthcare, security applications and sensing in the built and natural environments is prodigious.

Acknowledgements

This work was supported by an EPSRC Doctoral Training Centre grant (EP/G03690X/1).

Notes and references

‡ e.g. Sigma-Aldrich (Product Id: S067, CAS Number 9013-20-1 MDL number MFCD00082035)

‡ A total of 100 μL sample volume exposed to the surface (with 10 μL exposed at any one point in time) which, assuming perfect selective functionalisation of just the nanowires, has an functionalised surface area of $\sim 3\text{e}7 \text{ nm}^2$

† Gate area 10 μm^2 , $c_{\text{max}}=2 \text{ pM}$, analyte was exposed to the surface over two minutes, assuming all liquid came into contact with the surface (overestimate), at a flow rate of 300 $\mu\text{L}/\text{min}$ results in volume of 600 μL .

- 1 T. Vo-Dinh and B. Cullum, *Fresenius J. Anal. Chem.*, 2000, **366**, 540–551.
- 2 L. Senesac and T. G. Thundat, *Mater. Today*, 2008, **11**, 28–36.
- 3 P. Arora, A. Sindhu, N. Dilbaghi and A. Chaudhury, *Biosens. Bioelectron.*, 2011, **28**, 1–12.
- 4 J. Riu, A. Maroto and F. Rius, *Talanta*, 2006, **69**, 288–301.
- 5 A. Ramanavicius, F. W. Herberg, S. Hutschenreiter, B. Zimmermann, I. Lapėnaitė, A. Kaušaitė, A. Finkelšteinis and A. Ramanaviėienė, *Acta Medica Litua.*, 2005, **12**, 1–9.
- 6 S. G. Patching, *Biochim. Biophys. Acta BBA - Biomembr.*, 2014, **1838**, 43–55.
- 7 D. Cahen, R. Naaman and Z. Vager, *Adv. Funct. Mater.*, 2005, **15**, 1571–1578.
- 8 P. Bergveld, J. Wiersma and H. Meertens, *IEEE Trans. Biomed. Eng.*, 1976, **BME-23**, 136–144.
- 9 P. Bergveld, *IEEE Trans. Biomed. Eng.*, 1972, **BME-19**, 342–351.
- 10 P. Bergveld, *IEEE Trans. Biomed. Eng.*, 1970, **BME-17**, 70–71.
- 11 W. Oelßner, J. Zosel, U. Guth, T. Pechstein, W. Babel, J. G. Connery, C. Demuth, M. Grote Gansey and J. B. Verburg, *Sens. Actuators B Chem.*, 2005, **105**, 104–117.
- 12 M. J. Schöning and A. Poghossian, *Analyst*, 2002, **127**, 1137–1151.
- 13 M. J. Schöning and A. Poghossian, *Electroanalysis*, 2006, **18**, 1893–1900.
- 14 A. Nehra and K. Pal Singh, *Biosens. Bioelectron.*, 2015, **74**, 731–743.
- 15 G. Zheng, X. P. A. Gao and C. M. Lieber, *Nano Lett.*, 2010, **10**, 3179–3183.
- 16 S. Pud, J. Li, V. Sibiliev, M. Petrychuk, V. Kovalenko, A. Offenhäusser and S. Vitusevich, *Nano Lett.*, 2014, **14**, 578–584.
- 17 S. Chen, J. W. van Nieuwkastele, A. van den Berg and J. C. T. Eijkel, *Anal. Chem.*, 2016, **88**, 7890–7893.
- 18 K. Sun, I. Zeimpekis, C. Hu, N. M. J. Ditshego, O. Thomas, M. R. R. de Planque, H. M. H. Chong, H. Morgan and P. Ashburn, *Nanotechnology*, 2016, **27**, 285501.
- 19 R. E. G. Van Hal, J. C. T. Eijkel and P. Bergveld, *Sens. Actuators B Chem.*, 1995, **24**, 201–205.
- 20 P. Bergveld, *Sens. Actuators B Chem.*, 2003, **88**, 1–20.
- 21 H. Im, X.-J. Huang, B. Gu and Y.-K. Choi, *Nat. Nanotechnol.*, 2007, **2**, 430–434.
- 22 M. Im, J.-H. Ahn, J.-W. Han, T. J. Park, S. Y. Lee and Y.-K. Choi, *IEEE Sens. J.*, 2011, **11**, 351–360.
- 23 G. K. Iverson and J. C. Salmons, *J. Engl. Linguist.*, 2005, **33**, 207–221.
- 24 Y. Cheng, K.-S. Chen, N. L. Meyer, J. Yuan, L. S. Hirst, P. B. Chase and P. Xiong, *Biosens. Bioelectron.*, 2011, **26**, 4538–4544.
- 25 H. H. Liu, T. H. Lin and J.-T. Sheu, *Sens. Actuators B Chem.*, 2014, **192**, 111–116.
- 26 S. Chen and S.-L. Zhang, *Anal. Chem.*, 2011, **83**, 9546–9551.
- 27 N. Elfström, A. E. Karlström and J. Linnros, *Nano Lett.*, 2008, **8**, 945–949.
- 28 N. K. Rajan, X. Duan and M. A. Reed, *Wiley Interdiscip. Rev. Nanomed. Nanobiotechnol.*, 2013, **5**, 629–645.
- 29 I. Zeimpekis, K. Sun, C. Hu, N. M. J. Ditshego, O. Thomas, M. R. R. de Planque, H. M. H. Chong, H. Morgan and P. Ashburn, *Nanotechnology*, 2016, **27**, 165502.
- 30 A. Tarasov, W. Fu, O. Knopfmacher, J. Brunner, M. Calame and C. Schönenberger, *Appl. Phys. Lett.*, 2011, **98**, 012114.
- 31 Won Hee Lee, Jin-Moo Lee, Mihee Uhm, Jieun Lee, Kyung Rok Kim, Sung-Jin Choi, Dong Myong Kim, Yong-Joo Jeong and Dae Hwan Kim, *IEEE Electron Device Lett.*, 2014, **35**, 587–589.

- 32 S. Chen, L. Nyholm, N. Jokilaakso, A. E. Karlström, J. Linnros, U. Smith and S.-L. Zhang, *Electrochem. Solid-State Lett.*, 2011, **14**, J34–J37.
- 33 T. Rim, K. Kim, N. Hong, W. Ko, C.-K. Baek, S. Jeon, M. J. Deen, M. Meyyappan, Y.-H. Jeong and J.-S. Lee, *RSC Adv.*, 2013, **3**, 7963–7969.
- 34 X. Duan, Y. Li, N. K. Rajan, D. A. Routenberg, Y. Modis and M. A. Reed, *Nat. Nanotechnol.*, 2012, **7**, 401–407.
- 35 E. Stern, J. F. Klemic, D. A. Routenberg, P. N. Wyrembak, D. B. Turner-Evans, A. D. Hamilton, D. A. LaVan, T. M. Fahmy and M. A. Reed, *Nature*, 2007, **445**, 519–522.
- 36 Y. Cui, Q. Wei, H. Park and C. M. Lieber, *Science*, 2001, **293**, 1289–1292.
- 37 X. P. A. Gao, G. Zheng and C. M. Lieber, *Nano Lett.*, 2010, **10**, 547–552.
- 38 E. Buitrago, M. F.-B. Badia, Y. M. Georgiev, R. Yu, O. Lotty, J. D. Holmes, A. M. Nightingale, H. M. Guerin and A. M. Ionescu, *Sens. Actuators B Chem.*, 2014, **199**, 291–300.
- 39 J.-H. Ahn, S.-J. Choi, J.-W. Han, T. J. Park, S. Y. Lee and Y.-K. Choi, *Nano Lett.*, 2010, **10**, 2934–2938.
- 40 G. Shalev, G. Landman, I. Amit, Y. Rosenwaks and I. Levy, *NPG Asia Mater.*, 2013, **5**, e41.
- 41 M. O. Noor and U. J. Krull, *Anal. Chim. Acta*, 2014, **825**, 1–25.
- 42 S. Liu and X. Guo, *NPG Asia Mater.*, 2012, **4**, e23.
- 43 D. Sarkar, W. Liu, X. Xie, A. C. Anselmo, S. Mitragotri and K. Banerjee, *ACS Nano*, 2014, **8**, 3992–4003.
- 44 I. Heller, A. M. Janssens, J. Männik, E. D. Minot, S. G. Lemay and C. Dekker, *Nano Lett.*, 2008, **8**, 591–595.
- 45 I. Heller, J. Männik, S. G. Lemay and C. Dekker, *Nano Lett.*, 2009, **9**, 377–382.
- 46 T. E. Edmonds, in *Chemical Sensors*, Springer Science & Business Media, 2013, p. 223.
- 47 J. Janata, *The Analyst*, 1994, **119**, 2275.
- 48 X. Wen, S. Gupta, Y. Wang, T. R. N. Iii, S. C. Lee and W. Lu, *Appl. Phys. Lett.*, 2011, **99**, 043701.
- 49 X. Wen, S. Gupta, T. R. Nicholson, S. C. Lee and W. Lu, *Phys. Status Solidi C*, 2011, **8**, 2489–2491.
- 50 F. N. Ishikawa, M. Curreli, C. A. Olson, H.-I. Liao, R. Sun, R. W. Roberts, R. J. Cote, M. E. Thompson and C. Zhou, *ACS Nano*, 2010, **4**, 6914–6922.
- 51 N. K. Rajan, Yale University, 2013.
- 52 E. D. Minot, A. M. Janssens, I. Heller, H. A. Heering, C. Dekker and S. G. Lemay, *Appl. Phys. Lett.*, 2007, **91**, 093507.
- 53 U. Guth, F. Gerlach, M. Decker, W. Oelßner and W. Vonau, *J. Solid State Electrochem.*, 2009, **13**, 27–39.
- 54 M. Lambrechts and W. Sansen, in *Biosensors: Microelectrochemical Devices*, CRC Press, 1992, p. 69.
- 55 C. Toumazou and P. Georgiou, *Electron. Lett.*, 2011, **47**, S7–S12.
- 56 M. T. Martínez, Y.-C. Tseng, M. González and J. Bokor, *J. Phys. Chem. C*, 2012, **116**, 22579–22586.
- 57 Y. Taur and T. H. Ning, *Fundamentals of Modern VLSI Devices*, Cambridge University Press, Second Edition., 2013.
- 58 S. M. Sze, *Semiconductor Devices: Physics and Technology*, John Wiley & Sons, Inc., Hoboken, N.J., 2nd edition., 1985.
- 59 N. D. Arora, in *MOSFET Models for VLSI Circuit Simulation: Theory and Practice*, Springer Science & Business Media, 2012, p. 265.
- 60 A. Vacic and M. A. Reed, *J. Exp. Nanosci.*, 2014, **9**, 41–50.
- 61 R. J. Chen, H. C. Choi, S. Bangsaruntip, E. Yenilmez, X. Tang, Q. Wang, Y.-L. Chang and H. Dai, *J. Am. Chem. Soc.*, 2004, **126**, 1563–1568.
- 62 H. R. Byon and H. C. Choi, *J. Am. Chem. Soc.*, 2006, **128**, 2188–2189.
- 63 E. H. Williams, A. V. Davydov, A. Motayed, S. G. Sundaresan, P. Bocchini, L. J. Richter, G. Stan, K. Steffens, R. Zangmeister, J. A. Schreifels and M. V. Rao, *Appl. Surf. Sci.*, 2012, **258**, 6056–6063.
- 64 X. Duan, N. K. Rajan, M. H. Izadi and M. A. Reed, *Nanomed.*, 2013, **8**, 1839–1851.
- 65 S. Gupta, M. Elias, X. Wen, J. Shapiro, L. Brillson, W. Lu and S. C. Lee, *Biosens. Bioelectron.*, 2008, **24**, 505–511.
- 66 N. Clément, K. Nishiguchi, J. F. Dufreche, D. Guerin, A. Fujiwara and D. Vuillaume, *Appl. Phys. Lett.*, 2011, **98**, 014104.
- 67 A. Henning, M. Molotskii, N. Swaminathan, Y. Vaknin, A. Godkin, G. Shalev and Y. Rosenwaks, *Small*, 2015, **11**, 4931–4937.
- 68 G. Shalev, Y. Rosenwaks and I. Levy, *Biosens. Bioelectron.*, 2012, **31**, 510–515.
- 69 E. Buitrago, M. Fernández-Bolaños, Y. M. Georgiev, R. Yu, O. Lotty, J. D. Holmes, A. M. Nightingale and A. M. Ionescu, in *Proceedings of Technical Program - 2014 International Symposium on VLSI Technology, Systems and Application (VLSI-TSA)*, 2014, pp. 1–2.
- 70 S. Upadhyay, R. Frederiksen, N. Lloret, L. De Vico, P. Krogstrup, J. H. Jensen, K. L. Martinez and J. Nygård, *Appl. Phys. Lett.*, 2014, **104**, 203504.

- 71 R. A. Sperling and W. J. Parak, *Philos. Trans. R. Soc. Lond. Math. Phys. Eng. Sci.*, 2010, **368**, 1333–1383.
- 72 T. Sano and C. R. Cantor, *J. Biol. Chem.*, 1990, **265**, 3369–3373.
- 73 P. C. Weber, D. H. Ohlendorf, J. J. Wendoloski and F. R. Salemme, *Science*, 1989, **243**, 85–88.
- 74 N. Lloret, R. S. Frederiksen, T. C. Møller, N. I. Rieben, S. Upadhyay, L. D. Vico, J. H. Jensen, J. Nygård and K. L. Martinez, *Nanotechnology*, 2013, **24**, 035501.
- 75 N. A. Lapin and Y. J. Chabal, *J. Phys. Chem. B*, 2009, **113**, 8776–8783.
- 76 N. M. Green, in *Methods in Enzymology*, ed. M. W. and E. A. Bayer, Academic Press, 1990, vol. 184, pp. 51–67.
- 77 L. Chaiet and F. J. Wolf, *Arch. Biochem. Biophys.*, 1964, **106**, 1–5.
- 78 N. M. Green, in *Advances in Protein Chemistry*, ed. J. T. E. and F. M. R. C.B. Anfinsen, Academic Press, 1975, vol. 29, pp. 85–133.
- 79 S. Sivasankar, S. Subramaniam and D. Leckband, *Proc. Natl. Acad. Sci.*, 1998, **95**, 12961–12966.
- 80 Rockland Inc., *Streptavidin Properties and Characterization*, .
- 81 C. E. Argarana, I. D. Kuntz, S. Birken, R. Axel and C. R. Cantor, *Nucleic Acids Res.*, 1986, **14**, 1871–1882.
- 82 A. Pähler, W. A. Hendrickson, M. A. Kolks, C. E. Argaraña and C. R. Cantor, *J. Biol. Chem.*, 1987, **262**, 13933–13937.
- 83 L. Almonte, E. Lopez-Elvira and A. M. Baró, *ChemPhysChem*, 2014, **15**, 2768–2773.
- 84 R. C. Bruch and H. B. White, *Biochemistry (Mosc.)*, 1982, **21**, 5334–5341.
- 85 D. Wild, *The Immunoassay Handbook*, Gulf Professional Publishing, 2005.
- 86 M. D. Sonawane, S. B. Nimse, K.-S. Song and T. Kim, *RSC Adv*, 2016, **6**, 7599–7609.
- 87 A. Poghossian, A. Cherstvy, S. Ingebrandt, A. Offenhäusser and M. J. Schöning, *Sens. Actuators B Chem.*, 2005, **111–112**, 470–480.
- 88 E. J. Fogt, D. F. Untereker, M. S. Norenberg and M. E. Meyerhoff, *Anal. Chem.*, 1985, **57**, 1995–1998.
- 89 J. O. Bockris and A. K. N. Reddy, *Modern Electrochemistry 1*, Kluwer Academic Publishers, Boston, 1998, vol. 1.
- 90 B. N. Dominy, D. Perl, F. X. Schmid and C. L. Brooks III, *J. Mol. Biol.*, 2002, **319**, 541–554.
- 91 E. Stern, R. Wagner, F. J. Sigworth, R. Breaker, T. M. Fahmy and M. A. Reed, *Nano Lett.*, 2007, **7**, 3405–3409.
- 92 P. Bergveld, *Sens. Actuators Phys.*, 1996, **56**, 65–73.
- 93 H. H. Lee, M. Bae, S.-H. Jo, J.-K. Shin, D. H. Son, C.-H. Won and J.-H. Lee, *Sens. Mater.*, , DOI:10.18494/SAM.2015.1092.
- 94 P. Estrela, D. Paul, Q. Song, L. K. Stadler, L. Wang, E. Huq, J. J. Davis, P. K. Ferrigno and P. Migliorato, *Anal. Chem.*, 2010, **82**, 3531–3536.
- 95 P. Casal, X. Wen, S. Gupta, T. Nicholson, Y. Wang, A. Theiss, B. Bhushan, L. Brillson, W. Lu and S. C. Lee, *Philos. Trans. R. Soc. Math. Phys. Eng. Sci.*, 2012, **370**, 2474–2488.
- 96 A. Tarasov, M. Wipf, R. L. Stoop, K. Bedner, W. Fu, V. A. Guzenko, O. Knopfmacher, M. Calame and C. Schönenberger, *ACS Nano*, 2012, **6**, 9291–9298.
- 97 Y. Maekawa, Y. Shibuta and T. Sakata, *ChemElectroChem*, 2014, **1**, 1516–1524.
- 98 L. J. Criscenti, R. T. Cygan, A. S. Kooser and H. K. Moffat, *Chem. Mater.*, 2008, **20**, 4682–4693.
- 99 L. Bousse and P. Bergveld, *Sens. Actuators*, 1984, **6**, 65–78.
- 100 S. Jamasb, *IEEE Sens. J.*, 2004, **4**, 795–801.
- 101 S. Jamasb, S. Collins and R. L. Smith, *Sens. Actuators B Chem.*, 1998, **49**, 146–155.
- 102 S. Jamasb, S. D. Collins and R. L. Smith, in , 1997 *International Conference on Solid State Sensors and Actuators, 1997. TRANSDUCERS '97 Chicago, 1997*, vol. 2, pp. 1379–1382 vol.2.
- 103 S. Jamasb, S. D. Collins and R. L. Smith, *IEEE Trans. Electron Devices*, 1998, **45**, 1239–1245.
- 104 J.-L. Chiang, J.-C. Chou, Y.-C. Chen, G. S. Liau and C.-C. Cheng, *Jpn. J. Appl. Phys.*, 2003, **42**, 4973–4977.
- 105 S. Kim, D. W. Kwon, R. Lee, D. H. Kim and B.-G. Park, *Jpn. J. Appl. Phys.*, 2016, **55**, 06GG01.
- 106 B. S. Kang, F. Ren, L. Wang, C. Lofton, W. W. Tan, S. J. Pearton, A. Dabiran, A. Osinsky and P. P. Chow, *Appl. Phys. Lett.*, 2005, **87**, 023508.
- 107 Y. Wang, P. C. Sondergaard, A. Theiss, S. C. Lee and W. Lu, *ECS Trans.*, 2014, **61**, 139–146.
- 108 S. Jamasb, *Int. J. CIRCUITS Syst. SIGNAL Process.*
- 109 R. B. . Schasfoort, R. P. H. Kooyman, P. Bergveld and J. Greve, *Biosens. Bioelectron.*, 1990, **5**, 103–124.
- 110 P. Bergveld, *Biosens. Bioelectron.*, 1991, **6**, 55–72.
- 111 V. Krivitsky, M. Zverzhinetsky and F. Patolsky, *Nano Lett.*, 2016, **16**, 6272–6281.
- 112 S. Kim, J.-Y. Kim, J.-H. Ahn, T. J. Park, S. Y. Lee and Y.-K. Choi, *Appl. Phys. Lett.*, 2010, **97**, 073702.
- 113 N. Gao, W. Zhou, X. Jiang, G. Hong, T.-M. Fu and C. M. Lieber, *Nano Lett.*, 2015, **15**, 2143–2148.
- 114 K. Georgakopoulou, A. Birbas and C. Spathis, *J. Appl. Phys.*, 2015, **117**, 104505.

- 115 I. Jokić, M. Frantlović, Z. Djurić, K. Radulović and Z. Jokić, *Microelectron. Eng.*, 2015, **144**, 32–36.
- 116 G. S. Kulkarni and Z. Zhong, *Nano Lett.*, 2012, **12**, 719–723.
- 117 G. S. Kulkarni, W. Zang and Z. Zhong, *Acc. Chem. Res.*, 2016, **49**, 2578–2586.
- 118 M. Nič, J. Jiráť, B. Košata, A. Jenkins and A. McNaught, Eds., *IUPAC Compendium of Chemical Terminology: Gold Book*, IUPAC, Research Triangle Park, NC, 2.1.0., 2009.
- 119 F. N. Ishikawa, M. Curreli, H.-K. Chang, P.-C. Chen, R. Zhang, R. J. Cote, M. E. Thompson and C. Zhou, *ACS Nano*, 2009, **3**, 3969–3976.
- 120 H. Nam, B.-R. Oh, M. Chen, S. Wi, D. Li, K. Kurabayashi and X. Liang, *J. Vac. Sci. Technol. B Nanotechnol. Microelectron. Mater. Process. Meas. Phenom.*, 2015, **33**, 06FG01.
- 121 N. Elfström, Royal Institute of Technology, 2008.
- 122 R. L. Rich and D. G. Myszyka, *J. Mol. Recognit.*, 2008, **21**, 355–400.
- 123 S. Chen, J. G. Bomer, E. T. Carlen and A. van den Berg, *Nano Lett.*, 2011, **11**, 2334–2341.
- 124 K. Shoorideh and C. O. Chui, 2014, vol. 9174, pp. 917413-917413–6.
- 125 K. Shoorideh and C. O. Chui, *Proc. Natl. Acad. Sci.*, 2014, **111**, 5111–5116.
- 126 J. Lee, J. Jang, B. Choi, J. Yoon, J.-Y. Kim, Y.-K. Choi, D. M. Kim, D. H. Kim and S.-J. Choi, *Sci. Rep.*, 2015, **5**, 12286.
- 127 A. Vacic, J. M. Criscione, E. Stern, N. K. Rajan, T. Fahmy and M. A. Reed, in *2014 International Conference on Microelectronic Test Structures (ICMTS)*, 2014, pp. 203–206.
- 128 A. Vacic, J. M. Criscione, E. Stern, N. K. Rajan, T. Fahmy and M. A. Reed, *Biosens. Bioelectron.*, 2011, **28**, 239–242.
- 129 N. K. Rajan, K. Brower, X. Duan and M. A. Reed, *Appl. Phys. Lett.*, 2014, **104**, 084106.
- 130 N. K. Rajan, D. A. Routenberg and M. A. Reed, *Appl. Phys. Lett.*, 2011, **98**, 264107.
- 131 N. K. Rajan, D. A. Routenberg, J. Chen and M. A. Reed, *Appl. Phys. Lett.*, 2010, **97**, 243501.
- 132 M.-P. Lu, E. Vire and L. Montès, *Nanotechnology*, 2015, **26**, 495501.
- 133 Hyung-Kyu Lim and J. G. Fossum, *IEEE Trans. Electron Devices*, 1983, **30**, 1244–1251.
- 134 J. Go, P. R. Nair and M. A. Alam, *J. Appl. Phys.*, 2012, **112**, 034516.
- 135 J. Go, P. R. Nair, B. Reddy, B. Dorvel, R. Bashir and M. A. Alam, in *Electron Devices Meeting (IEDM), 2010 IEEE International*, 2010, p. 8.7.1-8.7.4.
- 136 O. Knopfmacher, A. Tarasov, W. Fu, M. Wipf, B. Niesen, M. Calame and C. Schönenberger, *Nano Lett.*, 2010, **10**, 2268–2274.
- 137 G. Shalev, A. Doron, U. Virobnik, A. Cohen, Y. Sanhedrai and I. Levy, *Appl. Phys. Lett.*, 2008, **93**, 083902.
- 138 H.-S. P. Wong, *IBM J. Res. Dev.*, 2002, **46**, 133–168.
- 139 K. Jayant, K. Auluck, M. Funke, S. Anwar, J. B. Phelps, P. H. Gordon, S. R. Rajwade and E. C. Kan, *Phys. Rev. E*, 2013, **88**, 012801.
- 140 K. Jayant, K. Auluck, M. Funke, S. Anwar, J. B. Phelps, P. H. Gordon, S. R. Rajwade and E. C. Kan, *Phys. Rev. E*, 2013, **88**, 012802.
- 141 K. Jayant, K. Auluck, S. Rodriguez, Y. Cao and E. C. Kan, *Phys. Rev. E*, 2014, **89**, 052817.
- 142 N. Elfström, R. Juhasz, I. Sychugov, T. Engfeldt, A. E. Karlström and J. Linnros, *Nano Lett.*, 2007, **7**, 2608–2612.
- 143 P. R. Nair and M. A. Alam, *IEEE Trans. Electron Devices*, 2007, **54**, 3400–3408.
- 144 H. Ghosh, D. Kundu and C. RoyChaudhuri, *IEEE Trans. Electron Devices*, 2016, **63**, 3241–3248.
- 145 J.-P. Colinge, *Silicon-on-Insulator Technology: Materials to VLSI: Materials to Vlsi*, Springer Science & Business Media, 2004.
- 146 P. R. Nair and M. A. Alam, *Appl. Phys. Lett.*, 2006, **88**, 233120.
- 147 P. E. Sheehan and L. J. Whitman, *Nano Lett.*, 2005, **5**, 803–807.
- 148 Y. Maekawa, Y. Shibuta and T. Sakata, *Chem. Phys. Lett.*, 2015, **619**, 152–157.
- 149 L. De Vico, L. Iversen, M. H. Sørensen, M. Brandbyge, J. Nygård, K. L. Martinez and J. H. Jensen, *Nanoscale*, 2011, **3**, 3635.
- 150 L. De Vico, M. H. Sørensen, L. Iversen, D. M. Rogers, B. S. Sørensen, M. Brandbyge, J. Nygård, K. L. Martinez and J. H. Jensen, *Nanoscale*, 2011, **3**, 706.
- 151 C. Heitzinger, N. J. Mauser and C. Ringhofer, *SIAM J. Appl. Math.*, 2010, **70**, 1634–1654.
- 152 P. R. Nair and M. A. Alam, *Nano Lett.*, 2008, **8**, 1281–1285.
- 153 S. Baumgartner, C. Heitzinger, A. Vacic and M. A. Reed, *Nanotechnology*, 2013, **24**, 225503.
- 154 T. Windbacher, V. Sverdlov, S. Selberherr, C. Heitzinger, N. Mauser and C. Ringhofer, in *AIP Conference Proceedings*, 2010, vol. 1199, p. 507.
- 155 M. W. Shinwari, M. J. Deen and D. Landheer, *Microelectron. Reliab.*, 2007, **47**, 2025–2057.
- 156 D. Landheer, W. R. McKinnon, W. H. Jiang and G. Aers, *Appl. Phys. Lett.*, 2008, **92**, 253901.

- 157 M. H. Sørensen, N. A. Mortensen and M. Brandbyge, *Appl. Phys. Lett.*, 2007, **91**, 102105–102105–3.
- 158 J. O. Bockris, A. K. N. Reddy and M. E. Gamboa-Aldeco, *Modern Electrochemistry 2A*, Kluwer Academic Publishers, Boston, 2002, vol. 2A.
- 159 A. Choi, K. Kim, H.-I. Jung and S. Y. Lee, *Sens. Actuators B Chem.*, 2010, **148**, 577–582.
- 160 P. Ginet, S. Akiyama, N. Takama, H. Fujita and B. Kim, *J. Micromechanics Microengineering*, 2011, **21**, 065008.
- 161 C.-Y. Hsiao, C.-H. Lin, C.-H. Hung, C.-J. Su, Y.-R. Lo, C.-C. Lee, H.-C. Lin, F.-H. Ko, T.-Y. Huang and Y.-S. Yang, *Biosens. Bioelectron.*, 2009, **24**, 1223–1229.
- 162 P. Hu, J. Zhang, Z. Wen and C. Zhang, *Nanotechnology*, 2011, **22**, 335502.
- 163 K. A. Jeon, H. J. Son, C. E. Kim, M. S. Shon, K. H. Yoo, A. M. Choi, H. I. Jung and Sang, *IEEE*, 2006, pp. 1265–1268.
- 164 J. S. Kim, W. I. Park, C.-H. Lee and G.-C. Yi, *Korean Phys. Soc.*, 2006, **49**, 1635.
- 165 D. Khatayevich, T. Page, C. Gresswell, Y. Hayamizu, W. Grady and M. Sarikaya, *Small*, 2014, **10**, 1505–1513.
- 166 I. R. Olmsted, A. Kussrow and D. J. Bornhop, *Anal. Chem.*, 2012, **84**, 10817–10822.
- 167 D. A. Hall and C. J. Langmead, *Br. J. Pharmacol.*, 2010, **161**, 1276–1290.
- 168 T. M. Squires, R. J. Messinger and S. R. Manalis, *Nat. Biotechnol.*, 2008, **26**, 417–426.
- 169 E. Stern, Yale University, 2007.
- 170 X. Duan, L. Mu, S. D. Sawtelle, N. K. Rajan, Z. Han, Y. Wang, H. Qu and M. A. Reed, *Adv. Funct. Mater.*, 2015, **25**, 2279–2286.
- 171 L. S. Jung, K. E. Nelson, P. S. Stayton and C. T. Campbell, *Langmuir*, 2000, **16**, 9421–9432.
- 172 D. Sarkar and K. Banerjee, *Appl. Phys. Lett.*, 2012, **100**, 143108.
- 173 M. L. Soudijn, University of Amsterdam, 2012.
- 174 C. J. T. de Grotthuss, *Ann Chim*, 1806, **58**, 54–73.
- 175 B. M. Lowe, C.-K. Skylaris and N. G. Green, *J. Colloid Interface Sci.*, 2015, **451**, 231–244.
- 176 P. Schuck and H. Zhao, *Methods Mol. Biol. Clifton NJ*, 2010, **627**, 15–54.
- 177 S. Kim, K. Kim, T. Rim, C. Park, D. Cho, C. K. Baek, Y. H. Jeong, M. Meyyappan and J. S. Lee, in *2011 IEEE International Conference on Nano/Micro Engineered and Molecular Systems (NEMS)*, 2011, pp. 1233–1236.
- 178 S. Kim, T. Rim, K. Kim, U. Lee, E. Baek, H. Lee, C.-K. Baek, M. Meyyappan, M. J. Deen and J.-S. Lee, *Analyst*, 2011, **136**, 5012–5016.
- 179 X. T. Vu, R. Stockmann, B. Wolfrum, A. Offenhäusser and S. Ingebrandt, *Phys. Status Solidi A*, 2010, **207**, 850–857.
- 180 C.-E. Lue, T.-C. Yu, C.-M. Yang, D. G. Pijanowska and C.-S. Lai, *Sensors*, 2011, **11**, 4562–4571.
- 181 A. Tarasov, N. de Rooij, C. Schönenberger and L. Linnros, University of Basel, 2012.
- 182 S. Zafar, C. D’Emic, A. Afzali, B. Fletcher, Y. Zhu and T. Ning, *Nanotechnology*, 2011, **22**, 405501.
- 183 S. Rigante, M. Wipf, A. Bazigos, K. Bedner, D. Bouvet and A. M. Ionescu, *IEEE*, San Francisco, CA, USA, 2014, pp. 1063–1066.
- 184 K. Bedner, V. A. Guzenko, A. Tarasov, M. Wipf, R. L. Stoop, D. Just, S. Rigante, W. Fu, R. A. Minamisawa, C. David and others, *Sens. Mater.*, 2013, **25**, 567–576.
- 185 E. Buitrago, École Polytechnique Fédérale de Lausanne, 2014.
- 186 T. Akiyama, Y. Ujihira, Y. Okabe, T. Sugano and E. Niki, *IEEE Trans. Electron Devices*, 1982, **29**, 1936–1941.
- 187 D. E. Yates, S. Levine and T. W. Healy, *J. Chem. Soc. Faraday Trans. 1 Phys. Chem. Condens. Phases*, 1974, **70**, 1807–1818.
- 188 T. W. Healy and L. R. White, *Adv. Colloid Interface Sci.*, 1978, **9**, 303–345.
- 189 A. Tarasov, M. Wipf, K. Bedner, J. Kurz, W. Fu, V. A. Guzenko, O. Knopfmacher, R. L. Stoop, M. Calame and C. Schönenberger, *Langmuir*, 2012, **28**, 9899–9905.
- 190 Meng-Nian Niu, Xin-Fang Ding and Qin-Yi Tong, *IEEE*, Penang, Malaysia, 1996, pp. 189–193.
- 191 A. Star, J.-C. P. Gabriel, K. Bradley and G. Grüner, *Nano Lett.*, 2003, **3**, 459–463.
- 192 R. L. Rich and D. G. Myszka, *J. Mol. Recognit.*, 2006, **19**, 478–534.
- 193 R. B. M. Schasfoort and A. J. Tudos, *Handbook of Surface Plasmon Resonance*, Royal Society of Chemistry, 2008.